The application of electromagnetic induction methods to reveal the hydrogeological structure of a riparian wetland

Authors:

Paul McLachlan[1], Guillaume Blanchy[1], Jonathan Chambers[2], James Sorensen[3], Sebastian Uhlemann[2,4], Paul Wilkinson[2], Andrew Binley[1].

Affiliations:

1 — Lancaster Environmental Centre, Lancaster University, LA1 4YQ, UK

2 — British Geological Survey, Keyworth, NG12 5GG, UK

3 — British Geological Survey, Wallingford, OX10 8ED, UK

4 — Lawrence Berkeley National Laboratory, Berkeley, CA 94720, US

ORCiD Numbers:

P. McLachlan - 0000-0003-2067-3790

G. Blanchy - 0000-0001-6341-5826

J. Chambers - 0000-0002-8135-776X

J. Sorensen - 0000-0002-2157-990X

S. Uhlemann - 0000-0002-7673-7346

P. Wilkinson - 0000-0001-6215-6535

A. Binley - 0000-0002-0938-9070

Corresponding Author:

P. McLachlan, p.mclachlan@outlook.com

Authorship Statement:

PM wrote the manuscript, and collected and modeled the data. All co-authors provided additional comments and ideas for the manuscript. Specifically, GB contributed to the development of inversion methodology. JC, JS, SU, and PW provided additional data and supervised project development, additionally, SU and JS aided in preliminary data collection. AB supervised project development and experimental design.

Highlights

- Raw *ECa* values are highly correlated with the thickness of alluvial soil in a riparian wetland.
- Alluvial soil thickness predictions from multi-linear regressions were more accurate than from EMI inversion methods.
- Robust predictions of hydraulic conductivity across the field site require more extensive intrusive data.

Declaration of Interest:

None

Abstract

Understanding ecologically sensitive wetlands often require non-invasive methods to characterize their complex structure (e.g. deposit heterogeneity) and hydrogeological parameters (e.g. hydraulic conductivity). Here, electrical conductivities of a riparian wetland were obtained using frequency-domain electromagnetic induction (EMI) methods. The wetland was previously characterized by extensive intrusive measurements and 3D electrical resistivity tomography (ERT) and hence offers an ideal opportunity to objectively assess EMI methods. Firstly, approaches to obtain structural information (e.g. elevation and thickness of alluvium) from EMI data and models were assessed. Regularized and sharp inversion algorithms were investigated for ERT calibrated EMI data. Moreover, the importance of EMI errors in inversion was investigated. The hydrological information content was assessed using correlations with piezometric data and petrophysical models. It was found that EMI data were dominated by the thickness of peaty alluvial soils and relatively insensitive to topography and total alluvial thickness. Furthermore, although error weighting in the inversion improved the accuracy of alluvial soil thickness predictions, the multi-linear regression method performed the best. For instance, an iso-conductivity method to estimate the alluvial soil thickness in the regularized models had a normalized mean absolute difference (*NMAD*) of *21.4%*, and although this performed better than the sharp inversion algorithm (*NMAD = 65.3%*), the multi-linear regression approach (using 100 intrusive observations) achieved a *NMAD = 18.0%*. In terms of hydrological information content, correlations between EMI results and piezometric data were poor, however robust relationships between petrophysically derived porosity and hydraulic conductivity were observed for the alluvial soils and gravels.

1 Introduction

The shallow subsurface structure of wetlands governs their ability to provide important hydrological and biogeochemical functions. For instance, the geometry of deposits and underlying bedrock, and their associated hydrogeological properties dictate the exchange of water, nutrients, and pollutants between surface waters and groundwaters. Prior to the 1970s, the importance of wetlands was commonly overlooked, and they were often modified for alternate land use, e.g. for agriculture or commercial and residential development (see Davidson, 2014). Since then there has been significant effort in restoring, maintaining, and managing wetlands (see Wagner et al., 2008). These efforts require methods for wetland characterization. However, conventional methods such as lithological sampling or piezometer installation (e.g. Grapes et al., 2005; Allen et al., 2010) may have limited spatial coverage or be prohibited due to any environmental damage they may cause.

Alternatively, hydrogeophysical methods provide the potential for subsurface characterization at high spatial and temporal resolutions (see reviews by Binley et al., 2015; Singha et al., 2015; McLachlan et al., 2017). Methods sensitive to electrical conductivity are of particular interest to wetland characterization as this property is dictated by porosity, pore water conductivity, saturation, grain mineralogy, and bulk density (e.g. Clement et al., 2020). These methods can therefore be used to distinguish between different lithologies and reveal hydrogeological parameters. The majority of hydrogeophysical wetland investigations use electrical resistivity tomography (ERT) due to their robust nature and ability to monitor dynamic processes (e.g. Slater and Reeve, 2002; Musgrave and Binley, 2011; Chambers et al., 2014; Miller et al., 2014; Walter et al., 2015; Uhlemann et al., 2016). However, recently the usage of frequency-domain electromagnetic induction (EMI) methods for wetland characterization has increased; this is in part due to the ease at which relatively large areas can be surveyed (e.g. von Hebel et al., 2014; Rejiba et al., 2018; Beucher et al., 2020). Furthermore, although the work here focusses on EMI methods it is worth noting that other geophysical methods have been employed successfully in similar wetland environments, e.g. ground penetrating radar has been used for structural characterization (Comas et al., 2005; Comas et al., 2011; Musgrave and Binley, 2011), estimation of gas content (Slater et al., 2007), and detection of peat pipes (Holden et al., 2003).

Initially, EMI methods were predominantly used for mapping (e.g. Sherlock and McDonnell, 2003; Corwin, 2008). For instance, variations in apparent conductivity (*ECa*) have been used to map water content (Corwin and Rhoades, 1984; Sherlock and McDonnell, 2003; Martini et al., 2017), clay content (Triantafilis and Lesch, 2005; Muzzamal et al., 2018) and soil organic matter (Huang et al., 2017). More recently, the developments of multi-coil and multi-frequency devices, and inversion algorithms (e.g. Monteiro-Santos, 2004; Auken et al., 2015; McLachlan et al., 2021), are such that applications have shifted focus to obtain quantitative models of electrical conductivity. In this way, EMI characterization can be two-fold: i.e. boundaries between contrasting electrical conductivity can be interpreted in terms of stratigraphy, and electrical conductivity can be converted to parameters of interest using petrophysical models. However, unlike ERT, EMI measurements can be influenced by several factors, e.g. device calibrations, user interference, and instrument drift.

As noted, there have been several studies using EMI inversion to investigate wetlands, peatlands, and fluvial environments. For instance, von Hebel et al. (2014) presented an inversion algorithm for sharp inversion (where conductivities and layer thicknesses were both solved as parameters) and Frederiksen et al. (2017) employed a smooth inversion algorithm and an iso-resistivity method for extracting lithological boundaries. Similar to Frederiksen et al. (2017), Boaga et al. (2020) used an iso-resistivity method and found that EMI data were able to resolve the boundary between peat and clay deposits with reasonable accuracy. In comparison, Beucher et al. (2020) used both sharp and smooth inversions but concluded that predictions from linear regressions with raw data were best for structural characterization when comparing with a limited intrusive data set. In addition to characterizing the subsurface structure, Brosten et al. (2010) investigated the link between EMI and hydraulic conductivity with a smooth inversion algorithm. The distinction between sharp and smooth inversion approaches is important, particularly in the case of 1D EMI inversions. For example, although electrical conductivity will vary smoothly in broadly homogenous units with varying water content or gradual changes in mineralogy, for distinctly stratified environments, regularisation in an inversion will smooth any abrupt changes in electrical conductivity. This becomes particularly problematic when building, or applying, petrophysical relationships to EMI data inverted using a smooth inversion as electrical signatures are likely to be damped substantially.

The overriding aim of this work is to assess the best modeling approaches to obtain information relevant to wetland function using EMI methods. The work focuses on a previously well-characterized site, where peaty alluvial soils and gravel deposits overlie a weathered Chalk bedrock. Firstly, the correlation between raw EMI measurements and structural properties (i.e. surface elevation, alluvial soil thickness, and total alluvial thickness) was assessed. Then the best approach for assessing the alluvial soil thickness was determined; predictions from multi-linear regressions and smooth and sharp inversion methods were validated against an extensive intrusive data set. For the inversions, EMI data were calibrated using ERT models, and measurement error was quantified by incorporating cross-over lines in the survey paths. For the multi-linear regression approach the number of intrusive observations required to build a robust relationship was investigated, to determine the minimum number of intrusive measurements required. Following this, the ability of EMI to characterize hydrogeological properties (i.e. unsaturated zone thickness as a proxy for pore water saturation, pore water conductivity, hydraulic conductivity, and porosity) was investigated by assessing correlations between piezometric data and using established petrophysical models. This work, therefore, provides a thorough investigation of the usage of EMI methods in wetland environments and provides insights for future work in similar, i.e. stratified, environments.

2 Methods

2.1 Field Site

The Boxford Wetland, West Berkshire, UK, covers an area of 10 ha and is situated along the River Lambourn. The river, and its associated habitats, are among the least impacted of the Chalk river systems in the UK; furthermore, the Boxford Wetland is a designated Site of Special Scientific Interest (Natural England) and a Special Area of Conservation (EU Habitats Directive) owing to the habitat it provides for aquatic and terrestrial fauna and flora (Old et al., 2014). The wetland consists of a north and a south meadow dissected by the Westbrook Channel (Fig. 1). Although minimally impacted, during the 18th century the hydrology of the site was modified by a network of drainage ditches, which are still evident in the topography of the site (Fig. 1b). Furthermore, some of these channels are coincident with the locations of groundwater-dependent flora and sites of groundwater upwelling (see Fig. 3 of House et al., 2015).

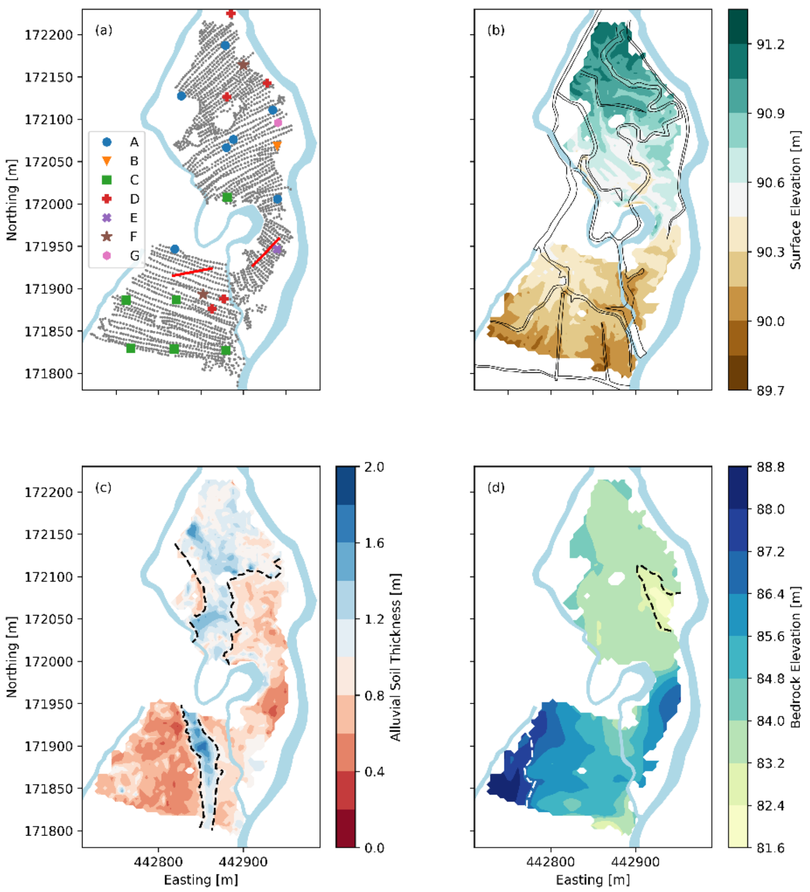

Figure 1 — Maps of (a) measurement location of alluvial soil thicknesses (grey dots), piezometers (symbols refer to the data available at each location, see supplementary information), and ERT transects (red lines), (b) topography, and 18th-century channels, (c) alluvial soil thickness and alluvium channel outline, and (d) thickness of superficial deposits from previous 3D ERT work (Chambers et al., 2014; Newell et al., 2015).

The underlying chalk bedrock present at the site is thought to exert a control on the hydrology (Chambers et al. 2014). This is primarily because the upper surface of the chalk is characterized by a discontinuous, low permeability, ‘putty chalk’ layer created by chemical weathering. Areas where the ‘putty chalk’ is absent or the chalk has been deeply eroded, e.g. the channel feature in the north meadow (see Fig. 1d), are thought to be areas of preferential groundwater upwelling (Younger et al., 1988; Chambers et al., 2014; House et al., 2016).

Overlying the chalk surface are Late Pleistocene to Holocene alluvial gravels and peaty alluvial soils. The geometries of these deposits were revealed by the 3D ERT survey of Chambers et al. (2014) who observed that the gravels were thicker (e.g. a total superficial thickness of 7 to 8 m) and more continuous in the north meadow than the south meadow where they thin to a thickness of around 1 m in the west (see Fig. 1d). A more detailed lithological study by Newell et al. (2015) demonstrated that the gravels can be divided into a unit of chalky gravels and an overlying unit of coarser flinty gravels, with some upper gravels showing the development of lateral accretion surfaces.

The alluvial soils comprise a heterogeneous mixture of peats, sands, clays, and silts (Chambers et al., 2014). Organic carbon analysis of the alluvial soils by Newell et al. (2016) indicated that they were deposited over 4,000 years ago and contain organic matter from both aquatic and terrestrial sources; i.e. the site was characterized by periodic changes in climate wetness. The complex depositional history of the alluvial soils is further evidenced by time-lapse ERT studies (Uhlemann et al. 2016; McLachlan et al., 2020), which demonstrated that they contain several hydrologically distinctive units. Most notably, the deposits comprise an upper and lower layer separated by a thin layer of clay. Both layers typically remain hydrologically separate and only exchange water when large hydraulic gradients are present, e.g. due to abrupt changes in the river stage and groundwater, which are strongly linked (Old et al., 2014).

2.2 Intrusive Data

The measured alluvial soil thicknesses (see Fig. 1a) used to assess correlations and validate the predictions from the EMI data here are from Chambers et al. (2014). Measurements involved pushing a 6 mm diameter steel rod into the subsurface. The gravel was assumed non-penetrable and the thicknesses were determined from the penetration depth of the rod. Measurements were made at 2815 locations on an approximate grid with 5 by 5 m spacing, see Chambers et al. (2014) for more details. Estimates of the depths to the chalk bedrock (i.e. total alluvial thickness) were taken from Newell et al. (2015) who combined the ERT data of Chambers et al. (2014) with additional intrusive information.

During the EMI and ERT field campaign (05-Mar-18 to 08-Mar-18), hydrological measurements were obtained from the alluvial soils and gravel piezometers at the site. In total 12, measurements of the unsaturated zone thickness in the alluvial soils and 13 measurements of pore water electrical conductivity were obtained from both the alluvial soils and gravels. The thickness of the unsaturated zone is taken here as a proxy for pore water saturation in the alluvial soils. Piezometers were purged twice to ensure that pore water conductivity measurements were representative. As the screens of many of the piezometers had become overgrown since their initial installation, a previous set of unpublished hydraulic conductivity measurements, obtained using the falling head method, were used for analysis. This included 19 hydraulic conductivity measurements for the gravels and 20 for the alluvial soils. The positions of piezometers are shown in Fig. 1a.

Additionally, as also noted by Beucher et al. (2020), there is interest in characterizing the organic matter content of peat-rich wetland sediments given their role in the global carbon cycles (see Mitsch and Gosselink, 2007). To address this, 24 auger cores of the alluvial soil were obtained across the site and subsampled into 0.1 m sections; organic matter content was then determined using the loss on ignition method (Heiri et al., 1999). Although a positive correlation between electrical conductivity and organic matter content may be expected given the surface conductivity component of organic sediments as observed by Comas and Slater (2004), here no significant relationships were found between raw or inverted EMI data and organic matter content. This is perhaps due to the high organic matter content of the alluvial deposits at the site and the limited variability between samples, i.e. organic carbon content is not the main driver of variability in bulk electrical conductivity. Consequently, these data are not discussed further.

2.3 Geophysical Data Collection

2.3.1 EMI Data Collection

EMI instruments measure the interaction between an induced primary electromagnetic field and the resultant secondary electromagnetic field. Here, EMI data were obtained using the GF Instruments CMD Explorer device (Brno, Czech Republic), hereafter referred to as the GF Explorer. This device contains three receiver coils with transmitter-receiver separation distances of 1.48, 2.82, and 4.49 m. Furthermore, it can be operated with coplanar coils orientated either vertically (VCP) or horizontally (HCP), with respect to the ground, meaning that in total 6 measurements can be obtained. Hereafter, the GF Explorer measurements are referred to as VCP1.48, VCP2.82, VCP4.49, HCP1.48, HCP2.82, and HCP4.49, to indicate the coil orientation and coil spacing.

In most cases, EMI devices like the GF Explorer are operated on, or near, the ground surface, however, at the field site, the presence of dense vegetation required that the device be manually carried at 1 m above ground level. This has implications for the depth sensitivity of the instrument. For instance, the depth of investigation values (i.e. the depth above which 70% of the signal comes from (see Callegary et al., 2007) for the specifications of the GF Explorer are 1.1, 2.2, and 3.4 m in VCP mode, or 2.1, 4.2, and 6.7 m in HCP mode when the device is operated at ground level. However, when operated at 1 m elevation the sensitivity patterns are shifted; following Andrade and Fischer (2018), the recalculated depth of investigation values become 2.7, 3.4, and 4.5 m for VCP mode, and 3.1, 4.6, and 6.9 m for HCP mode. Although the sensitivity patterns for VCP and HCP measurements are both shifted deeper, the effect is greater for VCP measurements. Essentially this means that when operated at 1 m elevation and assuming no sensitivity to above-ground features, the sensitivity patterns of the EMI measurements become more similar (i.e. less independent) and there is less sensitivity to the shallowest subsurface.

Before the field measurements, the GF Explorer was left for 30 minutes to allow it to stabilize. For each survey, the device was carried at 1 m and held perpendicularly to walking direction, transects were set approximately 5-10 m apart from each other. Furthermore, although in some places the ground was heavily vegetated, uneven, and/or boggy, care was taken to ensure that the GF Explorer remained in a stable position during surveying. For instance, changes in the height of the device, its orientation to the ground, and its rotation about its long axis will all have implications on the quality of measurements. To assess measurement quality, perpendicular survey lines were collected; this also enabled the assertation of whether any processing steps, e.g. drift corrections (as determined from a central drift station) or ERT calibration (see section 2.3.2) introduced any biases into the data. Measurements were logged every second and paired with coordinates obtained from a Trimble GPS (Sunnyvale, California, US) which has an accuracy of < 3 m; additionally, logged coordinates were shifted using 8 control points that were previously surveyed using a differential GPS.

2.3.2 ERT Data Collection

Although EMI devices provide an independent measure of electrical conductivity, several authors have advocated for calibrating EMI measurements before inversion (e.g. Lavoué et al., 2010; Minsley et al., 2013; von Hebel et al. 2014). Here, ERT data are used to calibrate EMI data following the same general approach of Lavoué et al. (2010); unlike EMI, ERT is not subject to drift or calibration issues. ERT methods use measurements of resistance collected using two pairs of electrodes; one pair to inject current and the other pair to measure the resultant electrical potential difference. By utilizing different combinations of electrodes with different spacings, different regions of the subsurface can be interrogated and a distribution of subsurface resistivity can be obtained via inverse modeling. It is important to note that the calibration of EMI data using ERT data implicitly assumes that the ERT model is correct, and any biases will be transferred into the EMI data. Also, the methods have different spatial resolutions, and ERT is sensitive to resistors whereas EMI is sensitive to conductors, which may also impart biases into the EMI data. Nonetheless, ERT calibration has been shown to aid with the convergence of EMI inversions (e.g. von Hebel et al., 2014; 2019).

Two ERT data sets were collected during the same period as the EMI data (i.e. 05-Mar-18 to 08-Mar-18), one in each meadow, (Fig. 1a). The locations of the ERT transects were selected to encompass ground with variable thicknesses of alluvial soil. Both transects were 47.5 m long and comprised 96 electrodes at 0.5 m spacing. Measurements were made using a dipole-dipole sequence and a Syscal Pro resistivity device (IRIS Instruments, Orleans, France). Before and following the collection of ERT data, plastic pegs, and string were used to mark the position of both transects to obtain EMI measurements in the same position as ERT measurements during respective surveys. Both data sets were inverted on a quadrilateral finite element mesh using R2 via the ResIPy software (Blanchy et al., 2020), and the depth of investigation was determined using the method proposed by Oldenburg and Li (1999).

2.4 EMI Data Filtering and Calibration

As the GF Explorer does not provide a measure of data quality in continuous logging mode, measurements that differed by more than 5% from both preceding and succeeding measurements were considered poor quality and replaced via linear interpolation to smooth the data. Following this, data were binned based on their *ECa* values into 16 equally spaced bins. Any data in bins that contained less than 0.5% of the total data were considered outliers, i.e. any extreme values were removed in this way. Data from each survey were then corrected based on measurements made at the drift station, this was done separately for each EMI data set.

The EMI measurements used for calibration were obtained during each survey; measurement coordinates were converted into a distance along the relevant ERT transect. The forward model response of each column of the quadrilateral ERT model was computed using the Maxwell-based forward models for each of the six measurement specifications of the GF Explorer. Each response was then converted to an *ECa* value using the low induction number approximation (see McNeill, 1980). To account for the different spatial resolutions of ERT and EMI methods, a running average across 3 samples (~1 m) was applied, and data were then binned based on their position along the ERT transect, for which bin widths of 1 m were used.

Additionally, the ERT depth of investigation, as computed by the Oldenburg and Li (1999) method, provided a metric by which to objectively avoid using EMI measurements obtained at locations along the ERT transect with poor depth sensitivity, e.g. at either end of the resistivity transect. Here, locations along the ERT transect where the depths of investigation were less than 1 m were not included. The coefficients from linear regressions for each measurement setup were then used to calibrate the remainder of the EMI data.

2.5 EMI Error Quantification

As noted, perpendicular survey lines, or cross-over lines, were collected to quantify errors within the data and determine if data processing had been effective. The errors were quantified by first locating cross-over points (i.e. locations of approximately perpendicular survey lines) within the VCP and HCP data sets. The mean and standard deviations were then computed for all measurements made within a two-meter radius of these cross-over points. By plotting the errors against time, it was evident that drift had been accounted for and no substantial errors were introduced by any of the processing steps (e.g. by drift correction or ERT calibration). The overall errors of the EMI data were low and showed a dependence on the magnitude (Fig. 2). For instance, expressed as a percentage the errors for VCP1.48, VCP2.82, VCP4.49, HCP1.48, HCP2.82, and HCP4.49 were 6.26, 3.72, 3.64, 3.30, 1.46, and 1.88%, respectively. These values are logical in that the measurements with the shallowest sensitivity patterns are characterized by higher errors. For instance, it could be anticipated that errors arising from orientation or elevation issues would be higher in higher conductivity regions of the wetland as the ratio of air to subsurface conductivity would be increased. Although this could explain why the measurements with a lower depth of investigation have higher errors, it is important to note that a similar effect could also arise from the variable vegetation cover at the site.

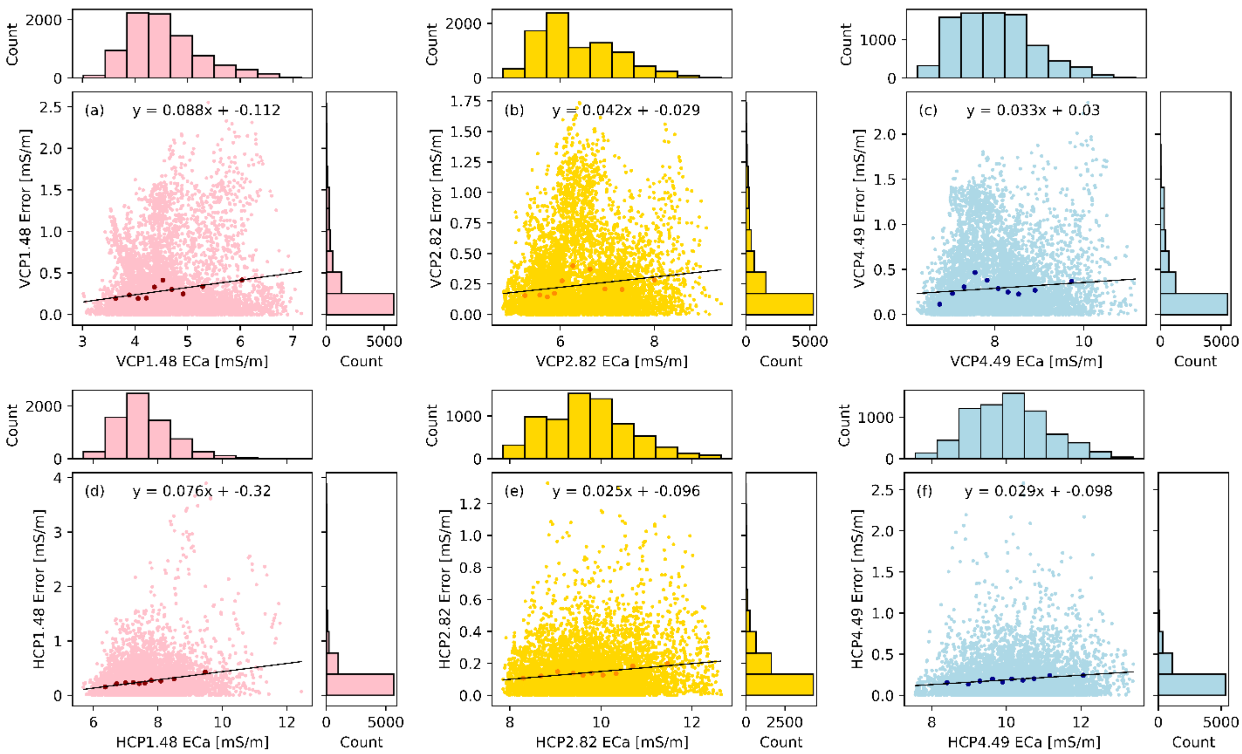

Figure 2 — Errors of EMI measurements show the relationship between *ECa* and error for (a) VCP1.48, (b) VCP2.82, (c) VCP4.49, (d) HCP1.48, (e) HCP2.82, and (f) HCP4.49 respectively.

2.6 EMI Inversion

Before inversion, EMI measurements were co-located by interpolating data onto the coordinates of the intrusive alluvial soil thickness measurements using inverse distance weighting. Only alluvial soil thickness measurement locations that had > 3 EMI measurements made within a 5 m radius were considered, this resulted in a co-located data set comprising 2308 measurements, out of the total 2815 alluvial soil thickness measurements collected. These data were inverted using the Maxwell-based forward models, as implemented in the open-source software EMagPy (McLachlan et al., 2021). As with other EMI inversion software the smooth inversion uses vertical regularisation to balance the overall data misfit and model smoothness. This avoids geologically unreasonable models at the expense of smoothing the electrical conductivity. In comparison, for the sharp inversion algorithm used here, regularization is not implemented, and depth to the interface is treated as a parameter. In both approaches the L2 norm was used, with the objective function, Φ, to be minimized:

$$\Phi = \frac{1}{N}\sum_{i=1}^{N}\left(d_i - f_i(m)\right)^2 + \alpha\frac{1}{M}\sum_{j=1}^{M-1}\left(\sigma_j - \sigma_{j+1}\right)^2 \tag{1}$$

where N is the number of measurements, d is the EMI data, $f(m)$ is the forward model response, α is the vertical smoothing, M is the number of model layers, and σ is the conductivity of each layer. For the sharp inversion, only the data misfit is considered, i.e. α is 0. Moreover, as noted, an approach to account for the error was also implemented for both the sharp and smooth inversions, this was achieved by dividing the data misfit by the normalized error as follows:

$$\Phi_d = \frac{1}{N}\sum_{i=1}^{N}\frac{\left(d_i - f_i(m)\right)^2}{\hat{\varepsilon}_i} \tag{2}$$

The smooth inversions were completed for an 11-layer model (depths = 0.2, 0.4, 0.6, 0.8, 1.0, 1.2, 1.4, 1.8, 2.4, 3 m) and an α value of 0.07. This approach assumes that beyond 3 m the subsurface is homogenous. However, in many cases, the boundary between the gravels and chalk was deeper (Fig. 1d). These depths were chosen because in most cases the conductivity profiles were monotonic, i.e. there was insufficient sensitivity to resolve the electrical properties of the chalk.

For the sharp inversions, a grid-based parameter search method (e.g. Dafflon et al., 2013) was used to produce two-layer models. This approach also assumes that the chalk and gravel were indistinguishable. This assumption is justified by the insignificant reduction in misfit when comparing 2 and 3-layer models, see Fig. 3. Additionally, the improvement in model convergence when data is calibrated can also be seen in Figure 3, e.g. the modal misfits are reduced from 8% to 3% following ERT calibration.

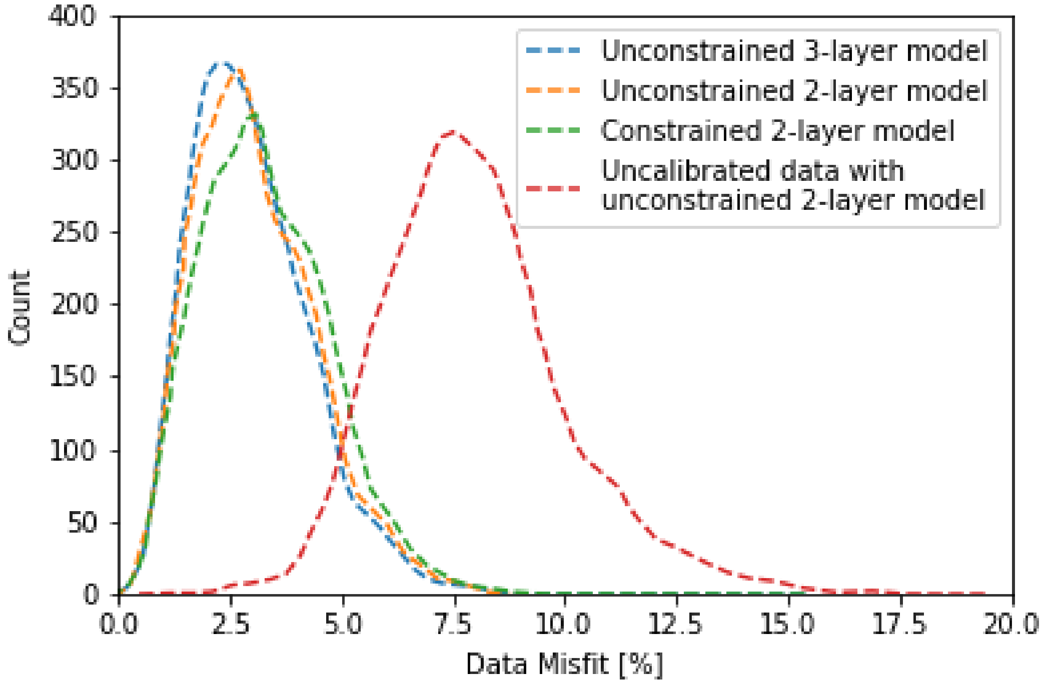

Figure 3 – Comparison of total misfit results for the inverted models for calibrated and uncalibrated data.

For the sharp, grid-based, inversion approach, values of 1 to 50 mS/m in 1 mS/m increments and 50 to 150 mS/m in 2 mS/m increments were used for the conductivities of layers 1 and 2. The parameters used for the thicknesses of layer 1 were 0.1 to 3 m in 0.1 m increments. The best model for each set of EMI measurements was determined from the lowest total data misfit. Moreover, any models with a data misfit of < 5% were retained to calculate the standard deviations of each parameter. Following this, to determine the effect of constraining the depth of layer 1 to the measured alluvial thickness, the model with the lowest misfit was then selected from the models with the correct alluvial thickness (rounded to nearest 0.1 m).

2.7 Structural Characterization

The correlations between the calibrated *ECa* measurements of each coil and the surface elevation, measured alluvial soil thickness, and total alluvial thickness (i.e. combined alluvial soil and gravel thickness) were assessed using linear regressions. Following this, alluvial soil thicknesses were estimated using a method where multi-linear regression models between the six EMI measurements and the alluvial soil thickness were built. Moreover, although the most robust multi-linear regression would be determined by using all the intrusive measurements, the interest here was in determining the minimum number of intrusive measurements needed to develop a model that characterizes alluvial soil thicknesses accurately, i.e. the point beyond which addition of intrusive data does not improve results. To do so multi-linear regressions were fitted with 20, 25, 30, 35, 45, 55, 65, 75, 85, 100, 150, 200, 250, 300, 400 and 500 randomly sampled sets of the co-located data. The resultant coefficients were then used to predict alluvial soil thickness for the remainder of the data set. To assess the ability of the linear regression to predict alluvial soil thickness the normalized mean absolute difference (*NMAD*) was determined by:

$$NMAD = \frac{\sum_{i=1}^{n}\left(\frac{|d_{meas,i} - d_{pred,i}|}{d_{pred,i}}\right)}{n} \tag{3}$$

where d_{meas} and d_{pred} are measured and predicted alluvial soil thicknesses and N is the number of observations. Furthermore, to ensure that predictions of the accuracy were robust, the multi-linear regressions were constructed 5,000 times for each subset using randomly sampled data.

Alluvial soil thicknesses were also estimated from the inverted EMI models. For the smooth models, the alluvial soil thicknesses were extracted using two classes of edge detection method: gradient and iso-surface methods. For the gradient method, the subsurface conductivity gradient was calculated, and the alluvial soil thickness was assumed to be the depth with the steepest gradient. For the iso-surface method, single values of conductivity were used to predict the alluvial soil thickness across the whole site. Additionally, the same analysis was carried out using resistivity values, but these did not perform as well. As with the linear regression method, the performance of gradient and iso-surface methods was assessed by calculating *NMAD*. For the sharp, grid-based parameter search method, the predicted alluvial soil thickness was simply taken as the thickness of the upper layer of the two-layer model for the cases where *a priori* knowledge of alluvial soil thickness was not supplied.

2.8 Hydrogeological Characterization

For the hydrogeological parameters, it was anticipated that there would be a negative correlation between EMI data and the unsaturated zone thickness, and a positive correlation with the pore water conductivity. For hydraulic conductivity, the expected correlation could be positive or negative. For instance, if the electrical conductivity is dictated by porosity, a positive correlation would be expected, whereas if the electrical conductivity is dictated by clay content a negative correlation would be anticipated (e.g. see Purvance and Adricevic, 2000).

As with the structural data, linear regressions between the calibrated *ECa* measurements of each coil and the hydrogeological data were first investigated. Following this, the correlations between the modeled electrical conductivities and the hydrogeological data were investigated. For the smooth models, conductivity values were determined for the alluvial soils and gravels by using the measured alluvial soil thicknesses to determine which model layers corresponded to the alluvial soils and which corresponded to the gravels. Although Brosten et al. (2011) selected a single model layer to correlate electrical conductivity with hydraulic conductivity such an approach requires, or at least assumes, that there is no thickness variation in the lithological units across the site. For both unconstrained and constrained sharp inversions, correlations between the hydrogeological properties of the alluvial soils and layer 1 were investigated, whereas the hydrological properties of the gravel were correlated with layer 2.

Additionally, modeled electrical conductivities were used to predict the porosity. Given that the gravels are fully saturated, and the surface conductivity can be assumed negligible, the porosity can be determined from Archie's (1942) law, as follows:

$$\sigma_b = \phi^m \sigma_w, \tag{4}$$

where σ_b is the bulk conductivity of the gravels, ϕ is the effective porosity, m is the cementation factor, here assumed to be 1.5, and σ_w is the pore water conductivity. For the alluvial soils, it is necessary to consider the influence of surface conductivity, on account of the organic matter and clay content. For this work, the surface conductivity contribution was estimated using data from the ERT monitoring work of Musgrave and Binley (2011) which also included local pore water electrical conductivity measurements from dip wells. Analysis of the data in Musgrave and Binley (2011) resulted in an estimated surface conductivity of 0.012 S/m, which is comparable to that of the peat deposits investigated in Comas and Slater (2004) when pore water electrical conductivities are similar to those at the Boxford field site, e.g. ~0.05 S/m. As with the gravels, the alluvial soils were assumed saturated such that:

$$\sigma_b = \Phi^m \sigma_w + \sigma_{surf}, \tag{5}$$

The assumption of saturation is an oversimplification as each piezometric measurement of the water table indicated that the alluvial soils were not fully saturated. However, preliminary inversions with the constraint of a sharp three-layer model with knowledge of the unsaturated zone thickness and alluvial soil thickness resulted in models with high electrical conductivity estimates of the unsaturated zone. This was in contrast with the anticipated lower saturation and could be attributed to a lack of sensitivity in this region or the presence of vegetation in regions modeled as infinitely resistive. Consequently, the alluvial soils were assumed saturated.

3. Results

ERT data

The ERT sections show a clear two-layer stratigraphy comprising a conductive upper layer and a more resistive lower layer (Fig. 4). Also, the measured alluvial soil thicknesses are coincident with this boundary. Consequently, the alluvial soil deposits have an average conductivity of 20–30 mS/m whereas the gravel has an average conductivity of 5-10 mS/m. This is in agreement with Chambers et al. (2014) who observed that the alluvial soils had a conductivity of ~30 mS/m in the north meadow ~20 mS/m in the south meadow, whereas the gravel had a conductivity of around 4–5 mS/m in both meadows. These values are in good agreement and the small deviation can be explained by the different seasons and years that the data were collected. Although Chambers et al. (2014) were able to resolve the underlying chalk with a conductivity of 6–8 mS/m, the Oldenburg and Li (1999) depth of investigation values here are relatively shallow and such a distinction was not possible. The superior depth sensitivity of Chambers et al. (2014) can be attributed to their larger electrode separation and larger survey scale.

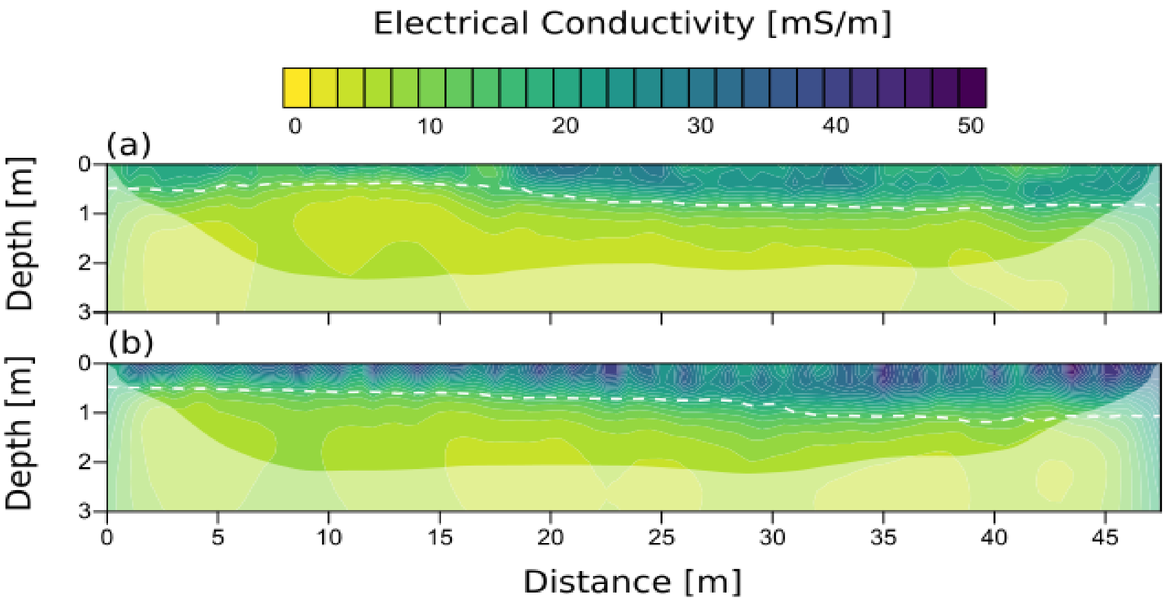

Figure 4 — ERT models of (a) north and (b) south meadow (see Fig. 1a for locations). Values are expressed in electrical conductivity; the white dashed line denotes the depth of the intrusively derived alluvial soil-gravel boundary. The depth of investigation is determined using the method proposed by Oldenburg and Li (1999), as implemented in ResIPy (Blanchy et al., 2020).

ECa data

The general patterns of EMI measured *ECa* coincide well with the alluvial soil thicknesses, e.g. the geometry of the north-south trending alluvial soil channel is expressed as a conductive anomaly in the *ECa* data (Fig. 5). Additionally, in the SW corner of the south meadow, the zone of elevated *ECa* is coincident with areas where the gravels are thin, i.e. the chalk bedrock is closer to the surface (Fig. 1d). It can also be seen in the north meadow that the zone of lower *ECa* values could correspond with the paleo-depression in the chalk surface identified from ERT results (Chambers et al., 2014; Newell, et al., 2015), although it is important to note here that the feature also corresponds to areas where the alluvial soils are thinnest. Lastly, although there were slight differences in the patterns of the *ECa* data for the different coil specifications they were all greater where the alluvial soils are thickest and smaller where the alluvial soils are thinnest.

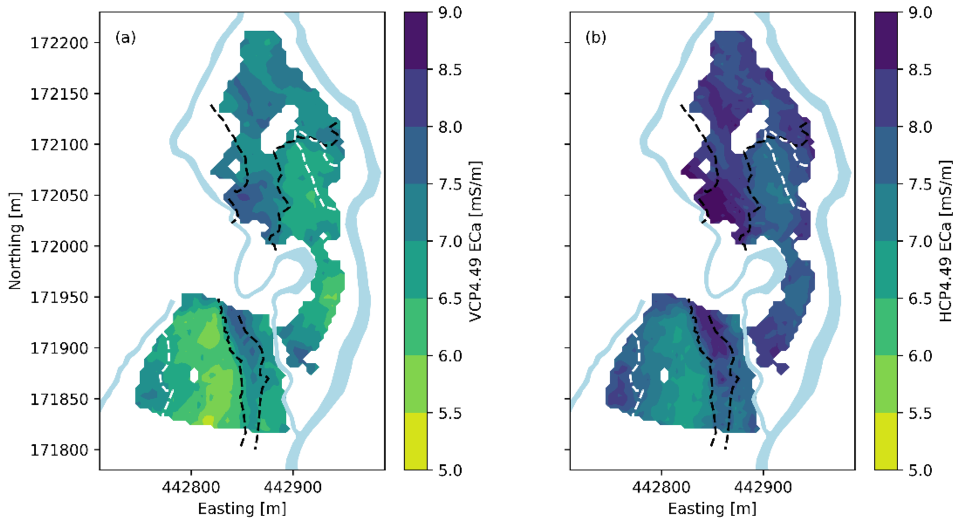

Figure 5 — Maps of *ECa* measurements from (a) VCP4.49 and (b) HCP2.82, depths of investigation are 4.5 and 4.6 m, respectively. The dashed lines denote the location of the intrusively derived alluvial soil-gravel boundary and the features of the gravel, see Fig. 1.

Structural Characterization

3.1.1 ECa and linear regression

The information of each GF Explorer measurement was quantified by fitting linear regressions between the calibrated *ECa* values and the available structural information, see Fig. 6. As expected from Fig. 5, it is evident that *ECa* measurements are primarily influenced by the alluvial soil thickness; the strongest correlations are for VCP4.49 and HCP2.82 (depth of investigation values are 4.5 and 4.6 m, respectively). Furthermore, although the other parameters show significant relationships, the correlation coefficient, *Pearson's r*, values are typically low to moderate. For instance, it could have been that EMI data were correlated with disturbance of the alluvial soils during the 18th century (e.g. Fig. 1b), however, EMI measurements were unable to resolve this. Moreover, although in some areas the gravel thicknesses agree with the EMI data (e.g. SE corner of the south meadow), this correlation is not present across the entire site and is likely only important when the alluvial soils are relatively thin.

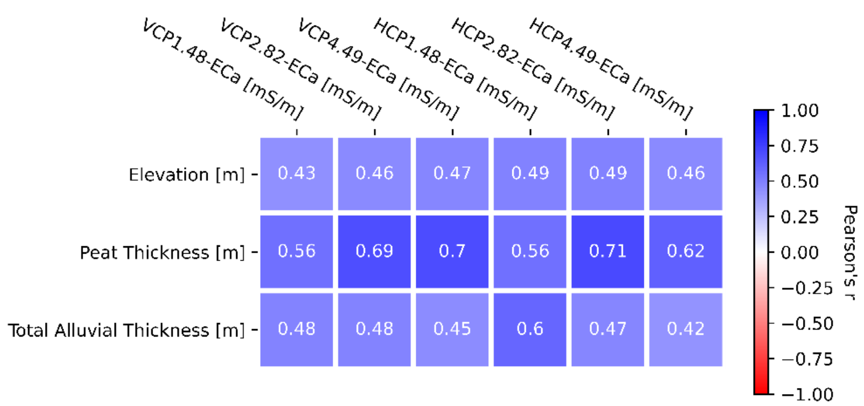

Figure 6 – Correlation plots of calibrated *ECa* measurements and structural information, in all

cases $n = 2308$ and $p < 0.01$. Total alluvial thickness corresponds to the thickness of both alluvial soils and gravels, i.e. the depth to the chalk bedrock.

It is shown in Fig. 7c that for multi-linear regressions using > 200 observations, the *NMAD* is not reduced substantially. For instance, in comparing the predictions from 200 and 400 observations, the average *NMAD* is only reduced from 17.5% to 17.3%. Furthermore, the predicted alluvial soil thickness from 100 intrusive measurements (see Fig. 7a) resolves the overall patterns of the alluvial soil thicknesses well and with reasonable accuracy (*NMAD = 18%*). However, it can be seen from Fig. 7b that areas where the alluvial soils are thickest are underestimated, and areas where the alluvial soils are thinnest are overestimated.

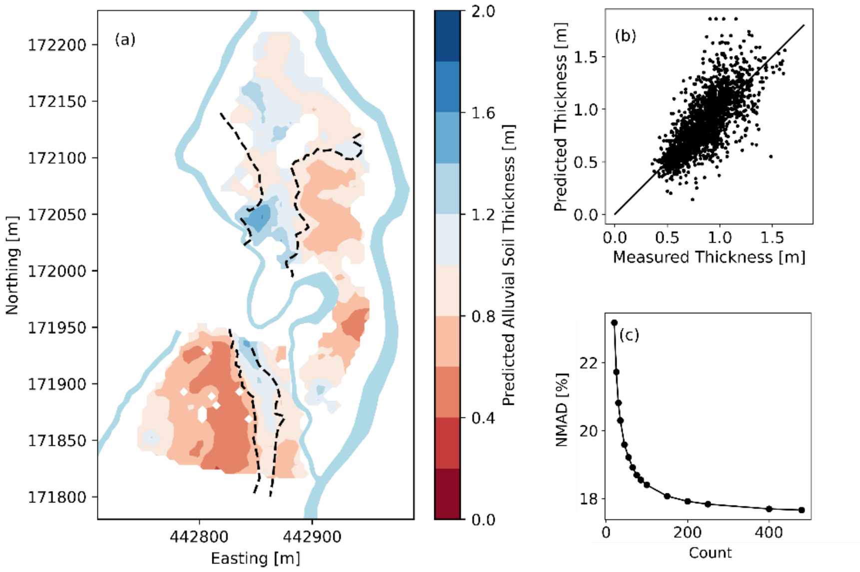

Figure 7 — Predicted alluvial soil thicknesses based on the linear regression: (a) shows the distribution of alluvial soil thicknesses, (b) shows the correlation between predicted and measured alluvial thicknesses, and (c) shows the improvement in terms of normalized mean absolute difference (*NMAD*) when more observations are included. The dashed lines in (a) indicate the location of the alluvial soil channel, also note that the color scale in (a) is the same as in Fig. 1b.

3.1.2 Smooth inversion and edge detection

Layer 3 (0.6 m depth) and Layer 9 (2.4 m depth) of the smooth inversion, where measurement error is included in the misfit calculation, are shown in Fig. 8a and b, respectively. As expected, the electrical conductivity decreases with depth, and the area corresponding to the alluvial channel occurs as a zone of elevated electrical conductivity. In terms of edge detection, it was found that the results from the models where error weighting was included were slightly better, for instance, the *NMAD* values for the iso-conductivity approach were 21.3% and 24.6% respectively. In comparison, the *NMAD* values for the conductivity gradient method were 44.3% and 44.6%, respectively. The predicted alluvial soil thickness, obtained by assuming the alluvial soil-gravel boundary can be represented by an iso-surface with a conductivity of 15.5 mS/m, is shown in Fig. 8c; the corresponding 1:1 plot is shown in Fig. 8d. Although the general pattern of the alluvial soil channel is well resolved, the predicted alluvial soil thicknesses were less accurate than the predictions from the multi-linear regression method. Moreover, the predictor performs poorer for thicker alluvial soil deposits, this could be attributed to the lower sensitivity (i.e. reduced model resolution) when the interface is at deeper depths.

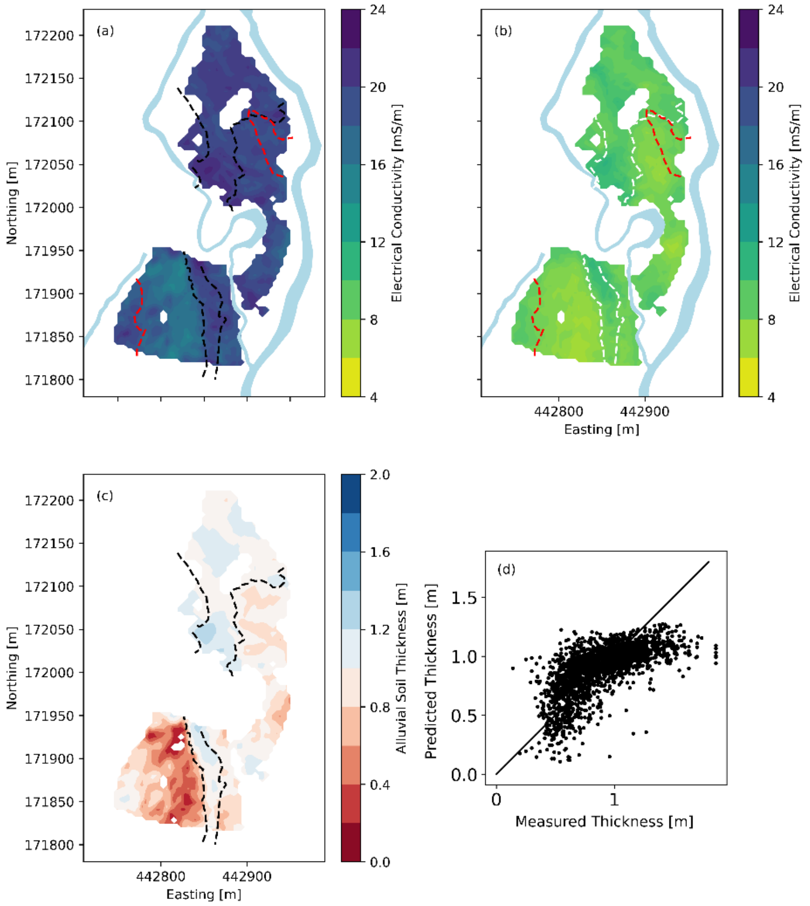

Figure 8 — Inverted electrical conductivity for smooth inversion: (a) and (b) show the inverted electrical conductivities of layers 3 (0.4 to 0.6 m) and 9 (1.8 to 2.4 m), respectively, (c) and (d) show the distribution of predicted alluvial soil thicknesses and a scatter plot of predicted and measured alluvial soil thicknesses, respectively. The dashed lines in (a), (b), and (c) indicate the location of the alluvial soil channel, also note that the color scale in (c) is the same as in Fig. 1b. -based parameter search

3.1.3 Grid-based parameter search

The results for the sharp model approach, where error weighting is used, are shown in Fig. 9a, b, and c. The general pattern of the alluvial soil thicknesses (Fig. 9c) is evident, however in most cases, the predicted alluvial soil thicknesses are overestimated, and the predictions have an *NMAD of 73.5%*. Furthermore, the conductivities of layer 1 (Fig. 9a) are correlated with the modeled alluvial soil thickness (*Pearson's r* = -0.88, $p < 0.01$); i.e. high conductivity regions occur where the depth of layer 1 is shallowest, and vice versa. This correlation is also evident in the electrical conductivities of layer 2 (Fig. 8b), although more subtle (*Pearson's* $r = -0.61$, $p < 0.01$). Such features imply that there is a high degree of non-uniqueness in the inversion solutions. This is further demonstrated in the standard deviations of parameters for each accepted model (i.e. data misfit < 5%), for instance for the error weighted inversion the mean standard deviations for the electrical conductivities of layers 1 and 2 were 23.17 mS/m and 14.18 mS/m, respectively, whereas the mean standard deviation for the thicknesses of layer 1 was 0.87 m. Moreover, the average standard deviations of layer conductivities are not substantially reduced when the thickness of layer 1 is constrained, with mean standard deviation values of 22.82 mS/m and 13.13 mS/m, respectively.

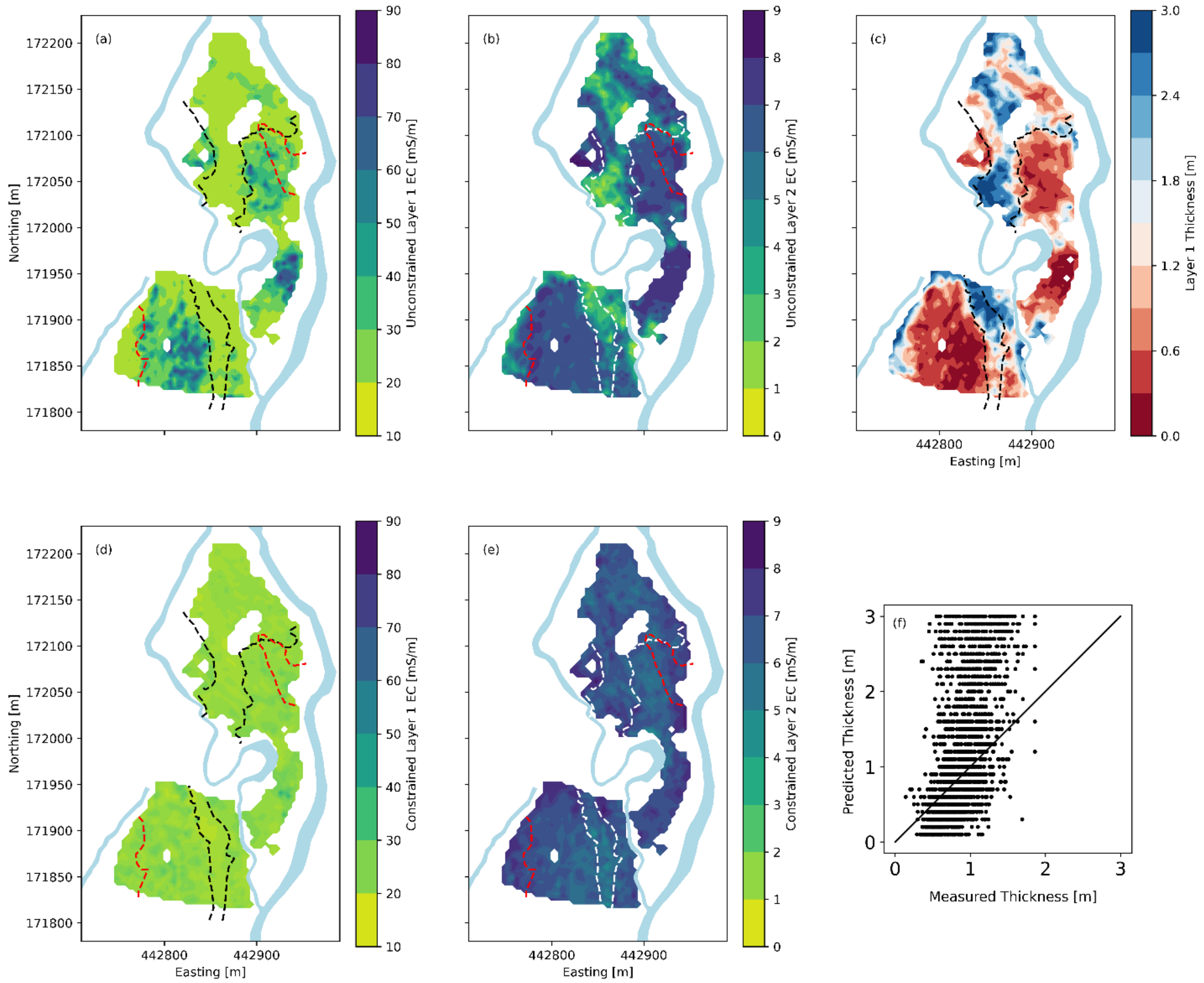

Figure 9 — Results of the sharp inversion approach for non-constrained and constrained cases with error weighting: (a), (b), and (c) show the layer 1 conductivities, layer 2 conductivities, and layer 1 depths of the unconstrained models. (d) and (e) show the electrical conductivities of layers 1 and 2 in the constrained approach. (f) shows the relationship between predicted and measured alluvial soil thickness. The dashed lines in (a), (b), and (c) indicate the location of the alluvial soil channel, also note that the color scale in (c) is the same as in Fig. 1b.

3.3. Hydrogeological Characterization

3.3.1 Correlation between EMI and hydrogeological observations

Fig. 10 displays the correlations between *ECa* measurements, inversion results, and hydrogeological parameters. It was anticipated that there would be negative correlations between *ECa* and thickness of the saturated zone; however, none of the correlations were statistically significant (at the 5%

level). Similarly, no significant relationships between *ECa* and the alluvial soil hydraulic conductivity, gravel hydraulic conductivity, or gravel water electrical conductivity were observed.

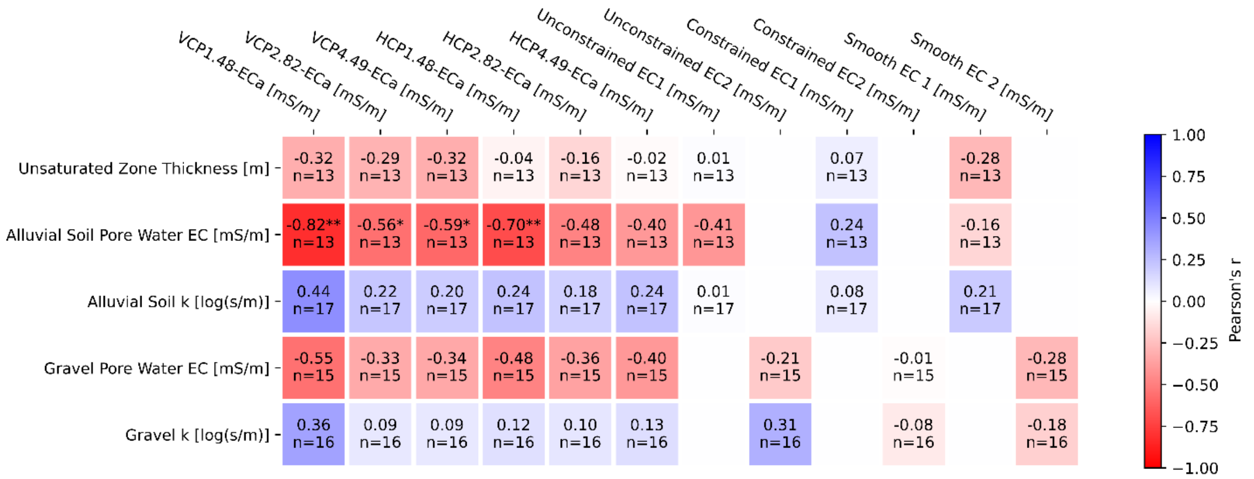

Figure 10 - Correlations between EMI measurements and hydrological parameters. Significance levels are indicated as follows: * represents $p < 0.05$ and ** represents $p < 0.01$.

Curiously, however, it was observed that all VCP measurements and HCP1.48 measurements had a significant negative correlation with alluvial soil pore water electrical conductivity. A possible explanation for this could be if porosity was negatively correlated with alluvial soil pore water electrical conductivity. For instance, areas with higher porosity may be flushed more readily by low conductivity rain waters. Such a hypothesis is somewhat backed by the correlation between alluvial soil water conductivity and log-transformed hydraulic conductivity of the alluvial soil *(r = -0.67, p < 0.05, n = 12*). Moreover, this phenomenon would be in line with the pore-dilation effect typically observed in peat-rich deposits (e.g. Ours et al., 1997; Kettridge and Binley, 2010).

However, it is important to note that the unconstrained layer 1 conductivity of the sharp inversion also displays a significant negative correlation. Given that such a correlation was not observed for the constrained sharp inversion, a negative correlation between pore-water electrical conductivity and alluvial soil thickness is also expected. It is however important to note the strongest relationships for peat pore-water electrical conductivity are with VCP1.48 and HCP1.48, whereas for alluvial soil thicknesses VCP4.49 and HCP2.82 had the strongest correlations, Fig 5.

3.3.2 Petrophysical characterization

The estimated porosities for the alluvial soils and gravels, following equations 4 and 5, and using the electrical conductivities from the error weighted constrained sharp inversions, resulted in mean porosities of 0.52 (SD = 0.08) and 0.30 (SD = 0.004), for the alluvial soils and gravels respectively. The porosity estimates for the gravels here agree with estimates of gravels in similar environments (e.g. Frings et al., 2011). It was also found that the estimated gravel porosities exhibited a significant positive correlation with hydraulic conductivity (*Pearson's r = 0.57, p < 0.05*), however for the alluvial deposits the correlation between porosity and hydraulic conductivity was weaker (*Pearson's r = 0.44, p < 0.05*). Nonetheless, given that pore water electrical conductivity values are required to obtain porosities, a petrophysical relationship to predict the hydraulic conductivity of gravels and alluvial soils across the site was not possible.

It is also worth noting that if the results from the smooth inversion are used to predict the porosities, the alluvial soils would have a mean estimated porosity of 0.21 and the gravels would have a mean estimated porosity of 0.51. This is because the true electrical contrast between gravels and alluvial soil is reduced in the smooth inversion, and although the electrical conductivities for the gravels are lower than the alluvial soil their higher estimated porosities are a result of the absence of the surface conductivity component in equation 4.

4. Discussion

4.1 Acquisition and Calibration of EMI Data

In this work, EMI data were collected at an elevation of 1 m due to the vegetation at the site. This has several important implications. Firstly, as noted, the sensitivity patterns of the device are modified. Although the exact modifications of the sensitivity patterns are dependent upon the subsurface conductivity, the approach investigated by Andrade and Fischer (2018) who use McNeill's (1980) cumulative sensitivity function, is validated by the observed similar correlations between alluvial soil thicknesses and VCP4.49 and HCP2.82 measurements, which have similar depth of investigation (4.6 and 4.5 m, respectively). Secondly, by elevating the device, the signal-to-noise ratio is reduced because the measurement magnitude is reduced, and the relative magnitude of errors is increased (e.g. device rotation or instability). Although some systematic errors are removed by ERT calibration, errors arising from acquisition errors or vegetation are still likely to influence the measurements and consequently the inversions. Furthermore, although using error weighting in the inversion did help to improve the model, the improvements were minimal.

Furthermore, although the factors mentioned above are likely to reduce the quality of data in similar environments, i.e. where vegetation precludes the use of all-terrain-vehicles and sleds, it is important to note that the walking survey here was still more productive than the 3D ERT investigation of Chambers et al. (2014). For instance, the EMI data collected here required 2-person-days to collect the data across the entire 10 ha field site, in comparison the work of Chambers et al. (2014) required 12-person-days. Furthermore, although the 3D ERT work provided superior characterization, the transport of numerous electrodes and cable spools may be unfeasible in remote sites and, if only shallow characterization is required, EMI offers a more attractive and rapid approach. ERT surveys are also more invasive (e.g. electrode placement and disturbance of vegetation), which can also be problematic in ecologically sensitive wetland environments.

In this work, data were calibrated using ERT models following the approach of Lavoué et al. (2011). Whilst it was observed that this substantially improved convergence of the EMI data (Fig. 3), it should be noted that the depths of investigation of the ERT survey, as determined by the Oldenburg and Li (1999) method, were substantially smaller than the depth of investigation of the EMI device. Depth of investigation could be improved by using a different electrode configuration (e.g. Wenner array) and/or larger electrode separations. Here a dipole-dipole sequence was chosen based on its ability to be optimized such that many data can be collected efficiently.

For the work here, due to the sensitivity of the ERT sections, the resultant calibration was essentially biased to the shallower subsurface, in comparison to the deeper areas; this is the opposite of Rejiba et al. (2018) who hypothesized that their choice of ERT set up did not allow accurate calibration of the shallowest subsurface. Moreover, although lateral smoothing was used to reduce artifacts related to different spatial resolution, these effects were not investigated in any significant detail. Future studies should investigate the influence of different quadrupole geometries and acquisition sequences in a more conclusive manner to assess the bias associated with ERT calibration.

Other methods to calibrate data, e.g. electrical resistivity sounding (von Hebel et al., 2019), soil sampling (e.g. Moghadas et al., 2012), and multi-elevation EMI measurements (e.g. Tan et al., 2019) have been investigated and may offer superior methods to calibration. It is clear, however, that an objective study investigating these approaches and the depth of investigation of electrical resistivity methods (which is seldom reported) could go a long way in ascertaining the best approach in the calibration of EMI data.

4.2 Predicting alluvial soil thickness using EMI methods

Although there is a range of EMI inversion software available, in this work EMagPy was used to produce smooth and sharp models of electrical conductivity. Ultimately, however, it was observed that the multi-linear regression method worked best. These findings agree with the recent work of Beucher et al. (2020) who found that the best approach for determining peat thickness was using a linear regression method and that it performed better than inverse models obtained from using the Aarhus workbench (Auken et al., 2008). Moreover, given that at low conductivity values the ERT calibration is assumed linear, bypassing the ERT calibration of the EMI data does not substantially reduce the performance of the multi-linear regression prediction method. For instance, using uncalibrated EMI data and 100 alluvial soil thickness observations yielded a relationship with an NMAD of 18.4%, in comparison to the NMAD of 18.0% when using calibrated data.

In this work, it is evident that the electrical conductivities of the unconstrained sharp inversion are highly correlated with the measured alluvial soil thickness, i.e. high first layer electrical conductivities are correlated with small first layer thicknesses. This is a crucial limitation of this approach, and although it could be argued that regularization could be introduced this may reduce the accuracy of petrophysical interpretations, e.g. overestimation of porosity in more resistive units or underestimation of porosity in more conductive units, as observed for the gravel and alluvial soils here. Potentially, the results of a non-regularized inversion could be improved by adding electrical conductivity bounds. For example, von Hebel (2014) proposed using bounds of double the maximum *ECa* value and half the minimum *ECa* value when the device was operated at ground level. Although this approach can be modified for cases where the device is elevated, such an approach would be too conservative to resolve the contrasting gravel and alluvial soil conductivities (as observed in the ERT results) at this field site. The failure of this method, i.e. high uncertainty in the final models, is likely a result of the underdetermined nature of the inverse problem, as although six measurements were obtained, they are noisy and are not truly independent. Furthermore, as noted, the similarity of measurements is increased by operating the device above the ground. For future applications retaining the lack of vertical regularization, the uncertainty of the inverse problem could perhaps be reduced by using lateral smoothing, collecting more measurements with different sensitivity patterns, or operating the device closer to the ground level.

Additionally, although the predictions using the smooth inversion were substantially better, they were not as good as the multi-linear regression method. This is likely due to a combination of regularization and discretization of the model which acts to smooth the boundaries. For instance, one could argue that given that as the inversions are conducted independently, it is not necessary to use the same vertical regularization and model discretization. Although this may improve alluvial soil thickness prediction, one cannot arbitrarily pick vertical smoothing values to obtain the best correlation. Nonetheless, it is possible that using an objective approach, such as an L-curve, could help to select independent vertical smoothing values for each 1D inversion. This however invokes a substantial increase in computation time, especially if full-Maxwell forward models are used.

4.3 Obtaining Hydrogeological Information

In addition to characterizing wetland structure, there is interest in obtaining hydrogeological information about wetlands. Given the dependence of EMI measurements on alluvial soil thickness, the data ought to be governed by contrasts in the hydrogeological properties between the alluvial soils and gravels. For instance, given the similarities of pore water conductivities at the time of sampling, the contrasts would most likely be linked to porosity and the presence of surface conductivity in the alluvial soils. Even in the case where structural information was supplied to the sharp inversion, the modeled electrical conductivities did not exhibit significant relationships with the hydrogeological information obtained from the piezometers. However, meaningful relationships between estimated porosity and log-transformed hydraulic conductivity were observed. Nonetheless, given that porosity estimates require knowledge of pore water conductivities it was not possible to estimate hydraulic conductivity across the field site. Although, if more data concerning the hydraulic conductivity and pore water conductivity were obtained it may be possible to make reasonable estimates of hydraulic conductivity across the field site.

As noted, when electrical conductivity values from the smooth inversion were used, the estimates for porosity were significantly lower than those obtained when using electrical conductivity values from the constrained sharp models. This has important implications for hydrogeological characterization because although site-specific relationships could be developed to link modeled electrical conductivity and hydrogeological parameters, any estimates will be highly dependent upon the regularization used in smooth inversions. Therefore, in stratified environments, the best approach would be to model data with a sharp inversion algorithm with structural constraint, e.g. ground-penetrating radar surveys have proved successful when vegetation cover does not preclude effective ground coupling (e.g. Slater and Reeve, 2002; Comas et al., 2004; Musgrave and Binley, 2011).

5 Conclusions and Outlook

EMI methods provide a productive method for characterizing the subsurface electrical conductivity. In this work, the potential of EMI methods to characterize the hydrogeological structure was assessed. EMI data were calibrated using ERT data and errors were quantified using cross-over points. Here the depth of investigation values of the ERT models were relatively shallow in comparison to the EMI sensitivity. Future applications ought to investigate the influence of differences in the vertical and spatial resolution between both methods. Moreover, although the inclusion of error weighting in the inversion improved the results, the improvements were minimal.

The calibrated EMI data were inverted using both smooth and sharp inversion algorithms, however, the absence of regularization in the sharp inversion resulted in large degrees of uncertainty in the resulting models. Such uncertainty could be reduced using intrusive information or the collection of more EMI measurements at each location. The smooth inversions permitted the characterization of the alluvial soil thickness relatively accurately, however, a method using the EMI data and a multi-linear regression model was superior in terms of accuracy. Moreover, the iso-conductivity measurement required the determination of a conductivity value; the robustness of selecting such a value was not investigated, as is done for the multi-linear regression approach. Additionally, in using the electrical conductivities obtained from the smooth models, the predicted alluvial porosities were likely underestimated whereas the gravel porosities were likely overestimated. Consideration of this is important for employing petrophysical models and establishing site-specific relationships.

Nonetheless, accurate characterization of the shallow structure is of clear benefit to wetland conceptualisation and management. Moreover, given that a multi-linear regression approach can be employed without the requirement for ERT calibration it provides a highly productive method for rapid characterization. Future investigations in similar sites where soil thicknesses are less than 2 m could easily be characterized by first collecting EMI data and then targeting different areas for intrusive sampling to build a multi-linear regression model for structural characterization.

Acknowledgements

This work was supported by the NERC Envision Doctoral Training Program (GA/15S/004 S301). We would like to thank Michael Tso and Tao Min for assistance in data collection. We are grateful to the constructive comments from the Associate Editor (Lee Slater) and Jacopo Boaga and an anonymous reviewer on an earlier version of the manuscript. The data used in this paper is accessible at the Lancaster University's research data repository https://doi.org/10.17635/lancaster/researchdata/468.

References

Allen, D.J., Darling, W.G., Gooddy, D.C. (2010). Interaction between groundwater, the hyporheic zone and a Chalk stream: a case study from the River Lambourn, UK. Hydrogeol J 18, 1125–1141. https://doi.org/10.1007/s10040-010-0592-2

Andrade, F., Fischer, T., Valenta, J. (2016). Study of Errors in Conductivity Meters Using the Low Induction Number Approximation and How to Overcome Them. 10.3997/2214-4609.201602080.

Andrade, F., Fischer, T. (2018). Generalised relative and cumulative response functions for electromagnetic induction conductivity meters operating at low induction numbers. Geophysical Prospecting. 66. 595-602. 10.1111/1365-2478.12553.

Archie, G.E. (1942). "The electrical resistivity log as an aid in determining some reservoir characteristics". Petroleum Transactions of AIME. 146: 54–62. doi:10.2118/942054-g.

Auken E. , Viezzoli A. Christensen A. (2009) A single software for processing, inversion, and presentation of AEM data of different systems: the Aarhus Workbench. *ASEG Extended*

Abstracts **2009**, 1-5.

Auken, E., Christiansen, A., Kirkegaard, C., Fiandaca, G., Schamper, C., Behroozmand, A., Binley, A., Nielsen, E., Efferso, F., Christensen, N., Sørensen, K., Foged, N., Vignoli, G. (2014). An overview of a highly versatile forward and stable inverse algorithm for airborne, ground-based and borehole electromagnetic and electric data. Exploration Geophysics. 10.1071/EG13097.

Beucher, A., Koganti, T., Iversen, B., Greve, M. (2020). Mapping of Peat Thickness Using a Multi-Receiver Electromagnetic Induction Instrument. Remote Sensing. 12. 21. 10.3390/rs12152458.

Binley, A., Hubbard, S. S., Huisman, J. A., Revil, A., Robinson, D. A., Singha, K., and Slater, L. D. (2015), The emergence of hydrogeophysics for improved understanding of subsurface processes over multiple scales, Water Resour. Res., 51, 3837– 3866, doi:10.1002/2015WR017016.

Blanchy, G., Saneiyan, S., Boyd, J., McLachlan, P., Binley, A. (2020) ResIPy, an intuitive open source software for complex geoelectrical inversion/modeling, Computers & Geosciences, Volume 137, 104423, ISSN 0098-3004, https://doi.org/10.1016/j.cageo.2020.104423.

Brosten, T., Day-Lewis, F., Schultz, G., Curtis, G., Lane, J. (2011). Inversion of multi-frequency electromagnetic induction data for 3D characterization of hydraulic conductivity. Journal of Applied Geophysics. 73. 323-335. 10.1016/j.jappgeo.2011.02.004.

Boaga, J., Viezzoli, A., Cassiani, G., Deidda, G. P., Tosi, L., Silvestri, Sonia. (2020). Resolving the thickness of peat deposits with contact-less electromagnetic methods: A case study in the Venice coastland. Science of The Total Environment. 737. 139361. 10.1016/j.scitotenv.2020.139361.

Callegary, J., Ferré, T., Groom, R. (2007). Vertical Spatial Sensitivity and Exploration Depth of Low-Induction-Number Electromagnetic-Induction Instruments. Vadose Zone Journal. 6. 158-167. 10.2136/vzj2006.0120.

Chambers, J., Wilkinson, P., Uhlemann, S., Sorensen, J., Roberts, C., Newell, A., Ward, W., Binley, A., Williams, P., Gooddy, D. (2014) Derivation of lowland riparian wetland deposit architecture using geophysical image analysis and interface detection. Water Resour Res 50:5886–5905

Clément, R., Pärn, J., Maddison, M., Henine, H. Chaumont, C., Tournebize, J., Uri, V., Espenberg, M., Günther, T., Mander, Ü. (2020). Frequency-domain electromagnetic induction for upscaling greenhouse gas fluxes in two hemiboreal drained peatland forests. Journal of Applied Geophysics. 173. 103944. 10.1016/j.jappgeo.2020.103944.

Comas, X., Slater, L., and Reeve, A. (2005), Geophysical and hydrological evaluation of two bog complexes in a northern peatland: Implications for the distribution of biogenic gases at the basin scale, Global Biogeochem. Cycles, 19, GB4023, doi:10.1029/2005GB002582.

Comas, Xavier & Slater, Lee. (2004). Low-frequency electrical properties of peat. Water Resources Research - Water Resour Res. 401. 10.1029/2004WR003534.

Corwin, D. (2008). Past, present, and future trends of soil electrical conductivity measurement using geophysical methods. Handbook of Agricultural Geophysics.

Corwin, D.L., Rhoades, J.D., 1984. Measurement of inverted electrical conductivity profiles using electromagnetic induction. Soil Sci. Soc. Am. J. 48 (2), 288–291.

Dafflon, B., Hubbard, S., Ulrich, C., Peterson, J.E. (2013), Electrical Conductivity Imaging of Active Layer and Permafrost in an Arctic Ecosystem, through Advanced Inversion of Electromagnetic Induction Data. Vadose Zone Journal, 12: 1-19 vzj2012.0161. doi:10.2136/vzj2012.0161

Davidson, N. (2014). How much wetland has the world lost? Long-term and recent trends in global wetland area. Marine and Freshwater Research. 65. 936-941. 10.1071/MF14173.

Frederiksen, R.,Christiansen, A., Christensen, S., Rasmussen, K. (2017). A direct comparison of EMI data and borehole data on a 1000 ha data set. Geoderma. 303. 188-195. 10.1016/j.geoderma.2017.04.028.

Grapes, T., Bradley, C., Petts, G. (2006). Hydrodynamics of floodplain wetlands in a chalk catchment: the River Lambourn, UK. Journal of Hydrology. 320 (3-4), pp. 324-341. https://doi.org/10.1016/j.jhydrol.2005.07.028

Heiri, O., Lotter, A., Lemcke, G. (2001) Loss on ignition as a method for estimating organic and carbonate content in sediments: reproducibility and comparability of results. Journal of Paleolimnology 25, 101–110 (2001). https://doi.org/10.1023/A:1008119611481

Holden, J., Burt, T., Vilas, M.. (2002). Application of ground-penetrating radar to the identification of subsurface piping in blanket peat. Earth Surface Processes and Landforms. 27. 10.1002/esp.316.

House, A. R., Thompson, J. R., Sorensen, J. P. R., Roberts, C., and Acreman, M. C. (2016) Modelling groundwater/surface water interaction in a managed riparian chalk valley wetland. Hydrol. Process., 30: 447– 462. doi: 10.1002/hyp.10625.

House, A.R., Thompson, J.R., Acreman, M.C. (2016). Projecting impacts of climate change on hydrological conditions and biotic responses in a chalk valley riparian wetland, Journal of Hydrology, Volume 534

House, A., Sorensen, J., Gooddy, D., Newell, A., Marchant, B., Mountford, J. Scarlett, P., Williams, P., Old, G. (2015). Discrete wetland groundwater discharges revealed with a three-dimensional temperature model and botanical indicators (Boxford, UK). Hydrogeology Journal. 23. 10.1007/s10040-015-1242-5.

Huang, J., Pedrera-Parrilla, A., Vanderlinden, K., Taguas, E.V., Gómez, J.A., Triantafilis, J., 2017a. Potential to map depth-specific soil organic matter contentacross an olive grove using quasi-2d and quasi-3d inversion of DUALEM-21 data. Catena 152 (May), 207–217. https://doi.org/10.1016/j.catena.2017.01.017.

Kettridge, N. and Binley, A. (2010), Evaluating the effect of using artificial pore water on the quality of laboratory hydraulic conductivity measurements of peat. Hydrol. Process., 24: 2629-

2640. https://doi.org/10.1002/hyp.7693

Lavoué, F., Kruk, J., Rings, J. Andre, F., Moghadas, D., Huisman, J., Lambot, S. Weihermüller, L., Vanderborght, J., Vereecken, H. (2010). Electromagnetic induction calibration using apparent electrical conductivity modelling based on electrical resistivity tomography. Near surface geophysics. 8. 553-561. 10.3997/1873-0604.2010037.

Martini, E., Werban, U., Zacharias, S., Pohle, M., Dietrich, P., Wollschläger, U., 2017. Repeated electromagnetic induction measurements for mapping soil moisture at the field scale: validation with data from a wireless soil moisture monitoring network. Hydrol. Earth Syst. Sci. 21 (1), 495–513. https://doi.org/10.5194/hess-21-495-

McLachlan, P., Blanchy, G., Binley, A., EMagPy: Open-source standalone software for processing, forward modeling and inversion of electromagnetic induction data, Computers & Geosciences, Volume 146, 2021,

McLachlan, P., Chambers, J., Uhlemann, S., Sorensen, J. and Binley, A. (2020), Electrical resistivity monitoring of river–groundwater interactions in a Chalk river and neighbouring riparian zone. Near Surface Geophysics, 18: 385-398. doi:10.1002/nsg.12114

McLachlan, P.J., Chambers, J.E., Uhlemann, S.S., et al. (2017) Geophysical Characterization of the Groundwater Surface Water Interface. Advances in Water Resources, 109, 302-319.

Mitsch, W., Bernal, B., Nahlik, A., Mander, Ü., Zhang, L., Anderson, C., ,Jørgensen, S., Brix, H. (2012). Wetlands, carbon, and climate change. Landscape Ecology. 28. 10.1007/s10980-012-9758-8.

Monteiro-Santos, F. A., (2004). 1-D laterally constrained inversion of EM34 profiling data. Journal of Applied Geophysics, 56(2), 123-134, doi:http://dx.doi.org/10.1016/j.jappgeo.2004.04.005.

Muzzamal, M., Huang, J., Nielson, R., Sefton, M., Triantafilis, J., 2018. Mapping soil particle-size fractions using additive log-ratio (ALR) and isometric log-ratio (ILR) transformations and proximally sensed ancillary data. Clay Clay Miner. 66, 9–27.

Newell, A., Sorensen, J., Chambers, J., Wilkinson, P., Uhlemann, S., Roberts, C., Gooddy, D., Vane, C., Binley, A.. (2015). Fluvial response to Late Pleistocene and Holocene environmental change in a Thames chalkland headwater: The Lambourn of southern England. Proceedings of the Geologists' Association. 126. 10.1016/j.pgeola.2015.08.008.

Newell, A., Vane, C., Sorensen, J., Moss-Hayes, V., Gooddy, D. (2016). Long-term Holocene groundwater fluctuations in a chalk catchment: evidence from Rock-Eval pyrolysis of riparian peats: Rock-Eval evidence for groundwater fluctuations in a chalk catchment. Hydrological Processes. 30. 10.1002/hyp.10903.

Old, G.H., Naden, P.S., Rameshwaran, P., Acreman, M.C., Baker, S., Edwards, F.K., Sorensen, J.P.R., 624 Mountford, O., Gooddy, D.C., Stratford, C.J., Scarlett, P.M., Newman, J.R., Neal, M., (2014). Instream 625 and riparian implications of weed cutting in a chalk river. Ecological

Engineering 71, 290-300

Oldenburg, D., Li. (1999) Estimating depth of investigation in dc resistivity and IP surveys GEOPHYSICS, 64(2):403

Ours, D. P., Siegel, D. I., Glaser, P. H. (1997) Chemical dilation and the dual porosity of humified bog peat, Journal of Hydrology, Volume 196, Issues 1–4, Pages 348-360.

Parsekian, A. D., Singha, K., Minsley, B. J., Holbrook, W. S.,, Slater, L. (2015), Multiscale geophysical imaging of the critical zone. Rev. Geophys., 53, 1– 26. doi: 10.1002/2014RG000465.

Sherlock, M.D., McDonnell, J.J. (2003), A new tool for hillslope hydrologists: spatially distributed groundwater level and soilwater content measured using electromagnetic induction. Hydrol. Process., 17: 1965-1977. doi:10.1002/hyp.1221

Singha, K., Day-Lewis, F. D., Johnson, T., Slater, L. D. (2015), Advances in interpretation of subsurface processes with time-lapse electrical imaging, Hydrol. Process., 29; pages 1549– 1576, doi: 10.1002/hyp.10280

Slater, L., Reeve A. (2002) Investigating peatland stratigraphy and hydrogeology using integrated electrical geophysics, Geophysics, 67, pg 365-378

Triantafilis, J., Lesch, S.M., 2005. Mapping clay content variation using electromagnetic induction techniques. Comput. Electron. Agric. 46 (1–3), 203–237.

Uhlemann, S.S., Sorensen, J. P. R., House, A. R., Wilkinson, P. B., Roberts, C., Gooddy, D. C., Binley, A. M., Chambers, J. E. (2016), Integrated time-lapse geoelectrical imaging of wetland hydrological processes, Water Resour. Res., 52, 1607– 1625, doi:10.1002/2015WR017932.

von Hebel, C., Rudolph, S., Mester, A., Huisman, J. A., Kumbhar, P., Vereecken, H., van der Kruk, J. (2014), Three-dimensional imaging of subsurface structural patterns using quantitative large-scale multiconfiguration electromagnetic induction data, Water Resour. Res., 50, 2732– 2748, doi:10.1002/2013WR014864.

von Hebel, C.; van der Kruk, J.; Huisman, J.A.; Mester, A.; Altdorff, D.; Endres, A.L.; Zimmermann, E.; Garré, S.; Vereecken, H. (2019). Calibration, Conversion, and Quantitative Multi-Layer Inversion of Multi-Coil Rigid-Boom Electromagnetic Induction Data. Sensors, 19, 4753.

Wagner, K., Gallagher, S., Hayes, M., Lawrence, B., Zedler, J. (2008). Wetland Restoration in the New Millennium: Do Research Efforts Match Opportunities?. Restoration Ecology. 16. 367 - 372. 10.1111/j.1526-100X.2008.00433.x.

Walter, J., Lück, E., Bauriegel, A., Richter, C. and Zeitz, J. (2015), Multi-scale analysis of electrical conductivity of peatlands for the assessment of peat properties. Eur J Soil Sci, 66: 639-650. doi:10.1111/ejss.12251

Whalley, W., Binley, A., Watts, C. (2017) Methods to estimate changes in soil water for phenotyping root activity in the field. Plant Soil 415, 407–422 https://doi.org/10.1007/s11104-016-3161-1

Younger,P. L. (1989) Devensian periglacial influences on the development of spatially variable permeability in the Chalk of southeast England Quarterly Journal of Engineering Geology and Hydrogeology, 22(4):343

Figure1.

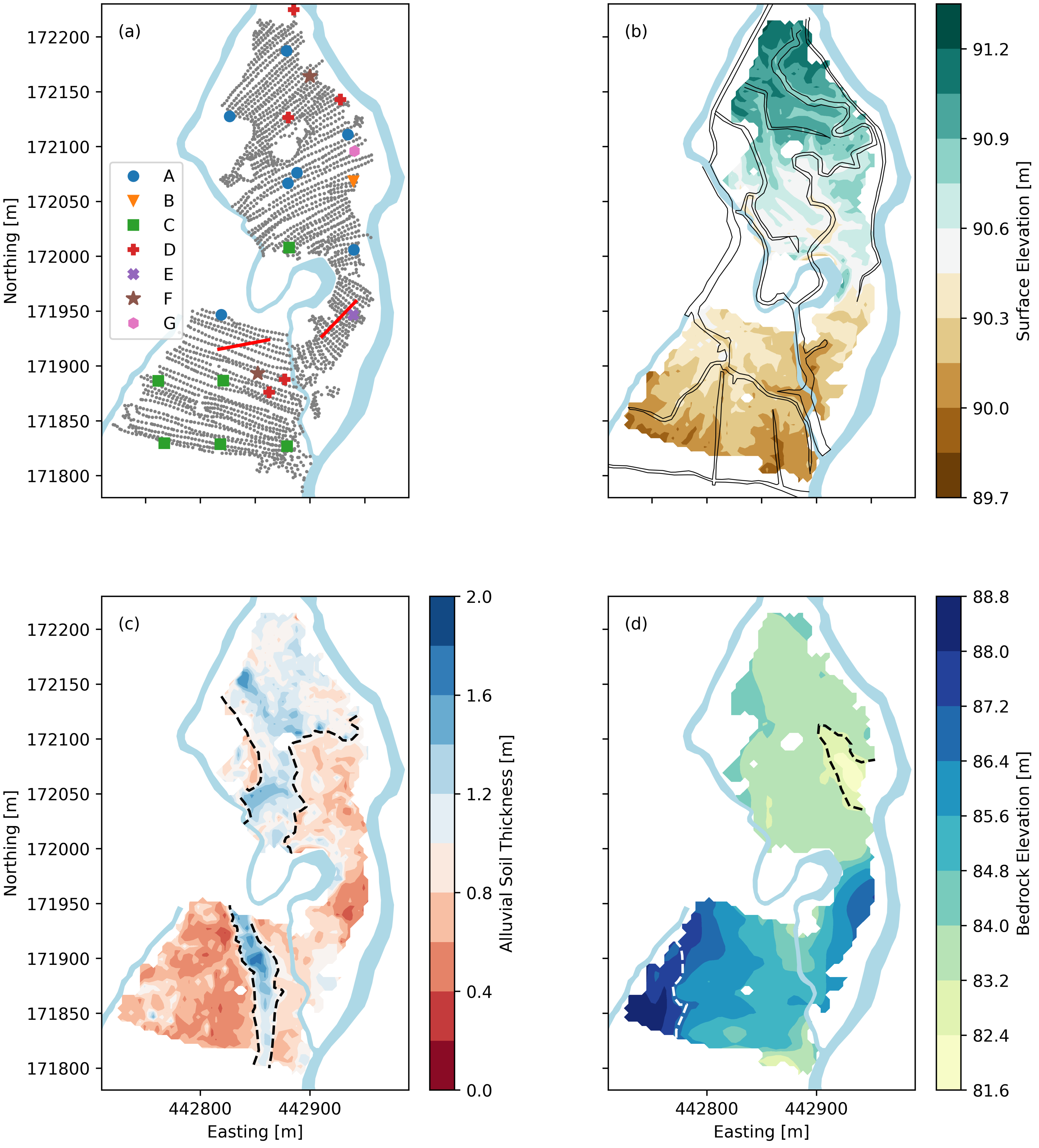
(a)
(b)
(c)
(d)
A
B
C
D
E
F
G
Northing [m]
Easting [m]
442800
442900
172200
172150
172100
172050
172000
171950
171900
171850
171800
Surface Elevation [m]
91.2
90.9
90.6
90.3
90.0
89.7
Alluvial Soil Thickness [m]
2.0
1.6
1.2
0.8
0.4
0.0
Bedrock Elevation [m]
88.8
88.0
87.2
86.4
85.6
84.8
84.0
83.2
82.4
81.6

Figure2.

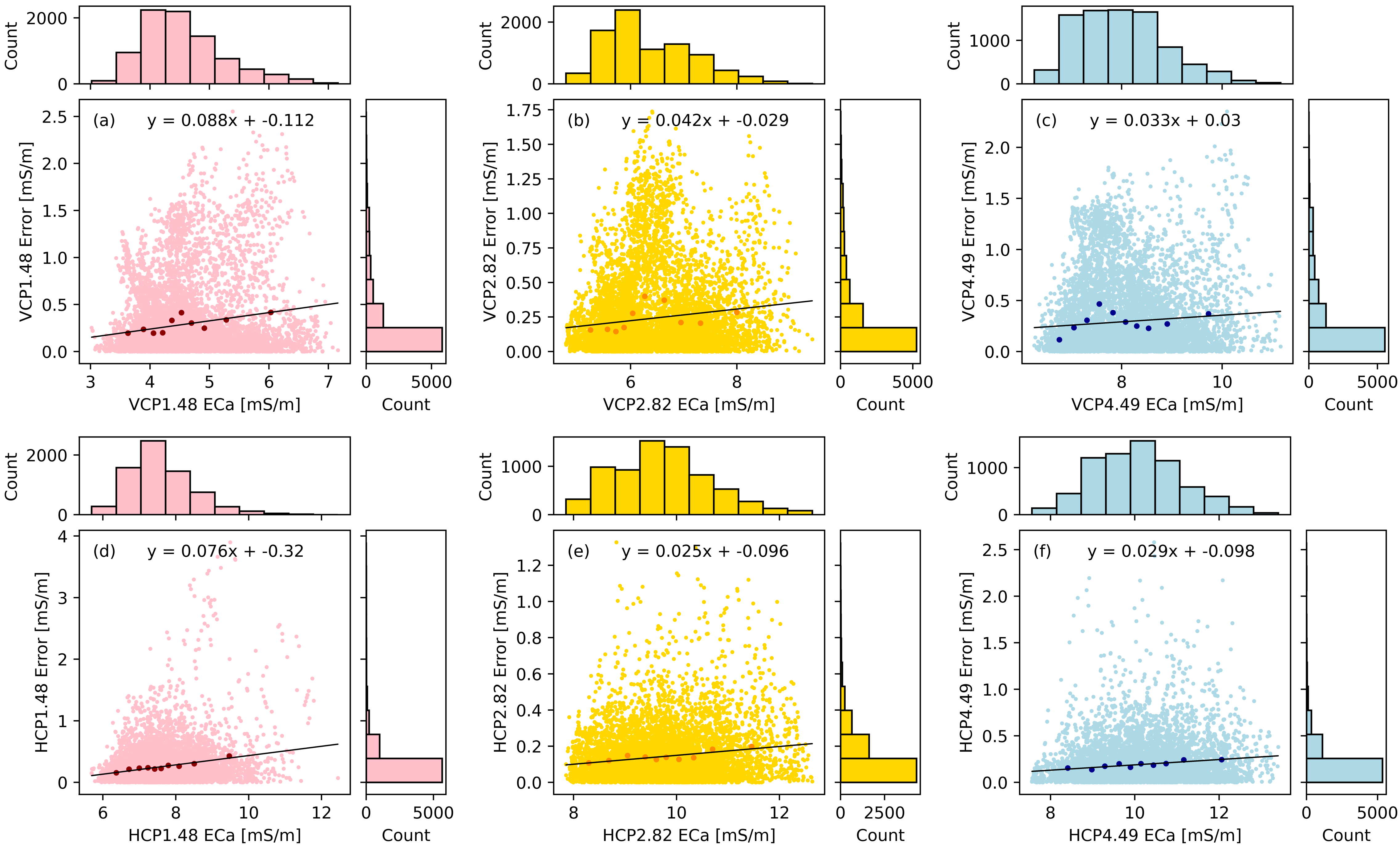

(a) y = 0.088x + -0.112
VCP1.48 Error [mS/m]
VCP1.48 ECa [mS/m]
(b) y = 0.042x + -0.029
VCP2.82 Error [mS/m]
VCP2.82 ECa [mS/m]
(c) y = 0.033x + 0.03
VCP4.49 Error [mS/m]
VCP4.49 ECa [mS/m]
(d) y = 0.076x + -0.32
HCP1.48 Error [mS/m]
HCP1.48 ECa [mS/m]
(e) y = 0.025x + -0.096
HCP2.82 Error [mS/m]
HCP2.82 ECa [mS/m]
(f) y = 0.029x + -0.098
HCP4.49 Error [mS/m]
HCP4.49 ECa [mS/m]
Count

Figure3.

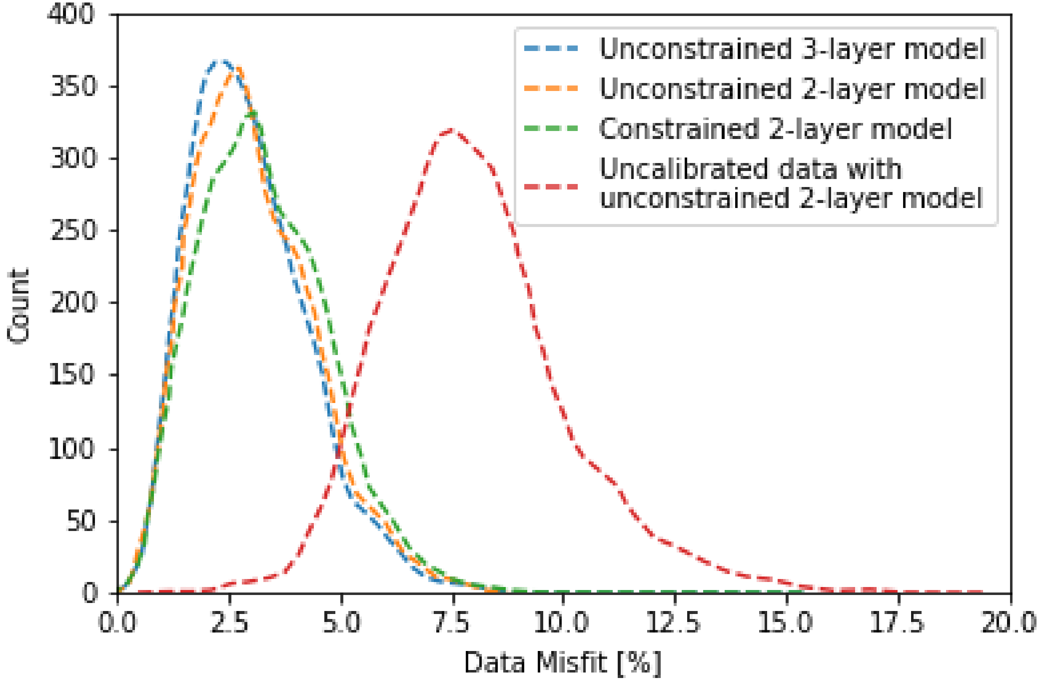
Unconstrained 3-layer model
Unconstrained 2-layer model
Constrained 2-layer model
Uncalibrated data with unconstrained 2-layer model
Count
Data Misfit [%]
0
50
100
150
200
250
300
350
400
0.0
2.5
5.0
7.5
10.0
12.5
15.0
17.5
20.0

Figure4.

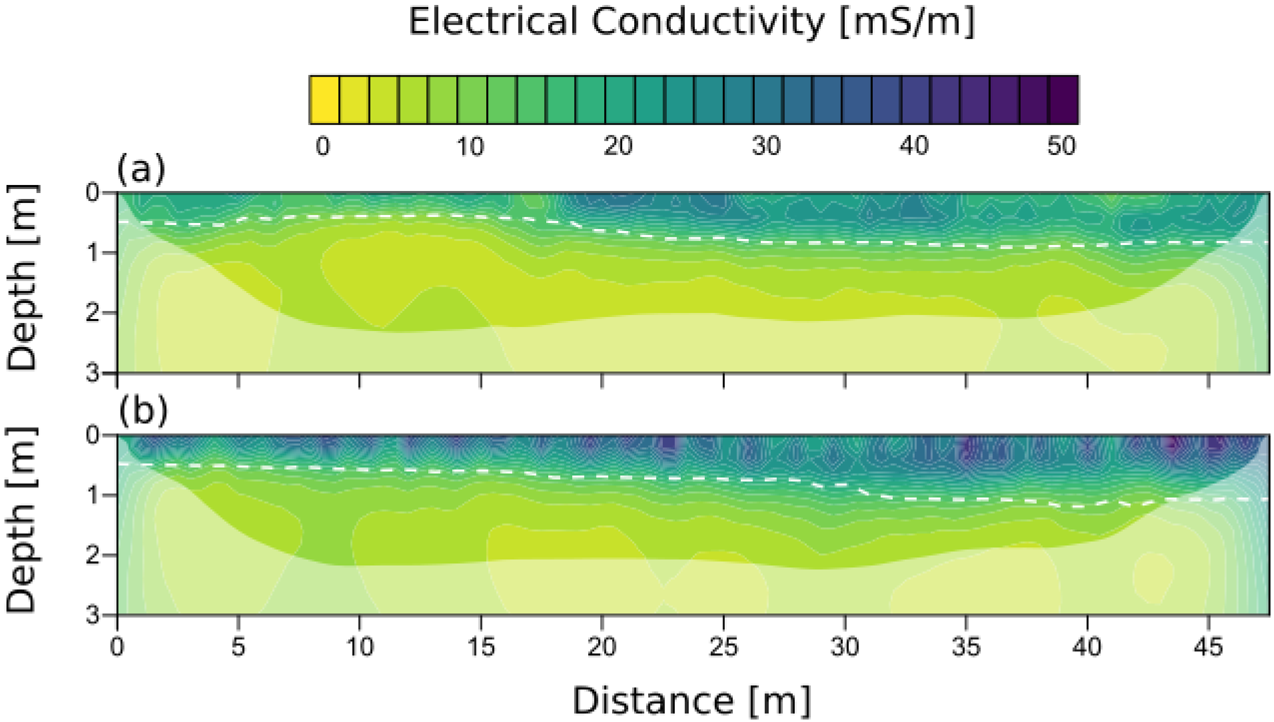

Electrical Conductivity [mS/m]
0
10
20
30
40
50
(a)
Depth [m]
0
1
2
3
(b)
Depth [m]
0
1
2
3
0
5
10
15
20
25
30
35
40
45
Distance [m]

Figure5.

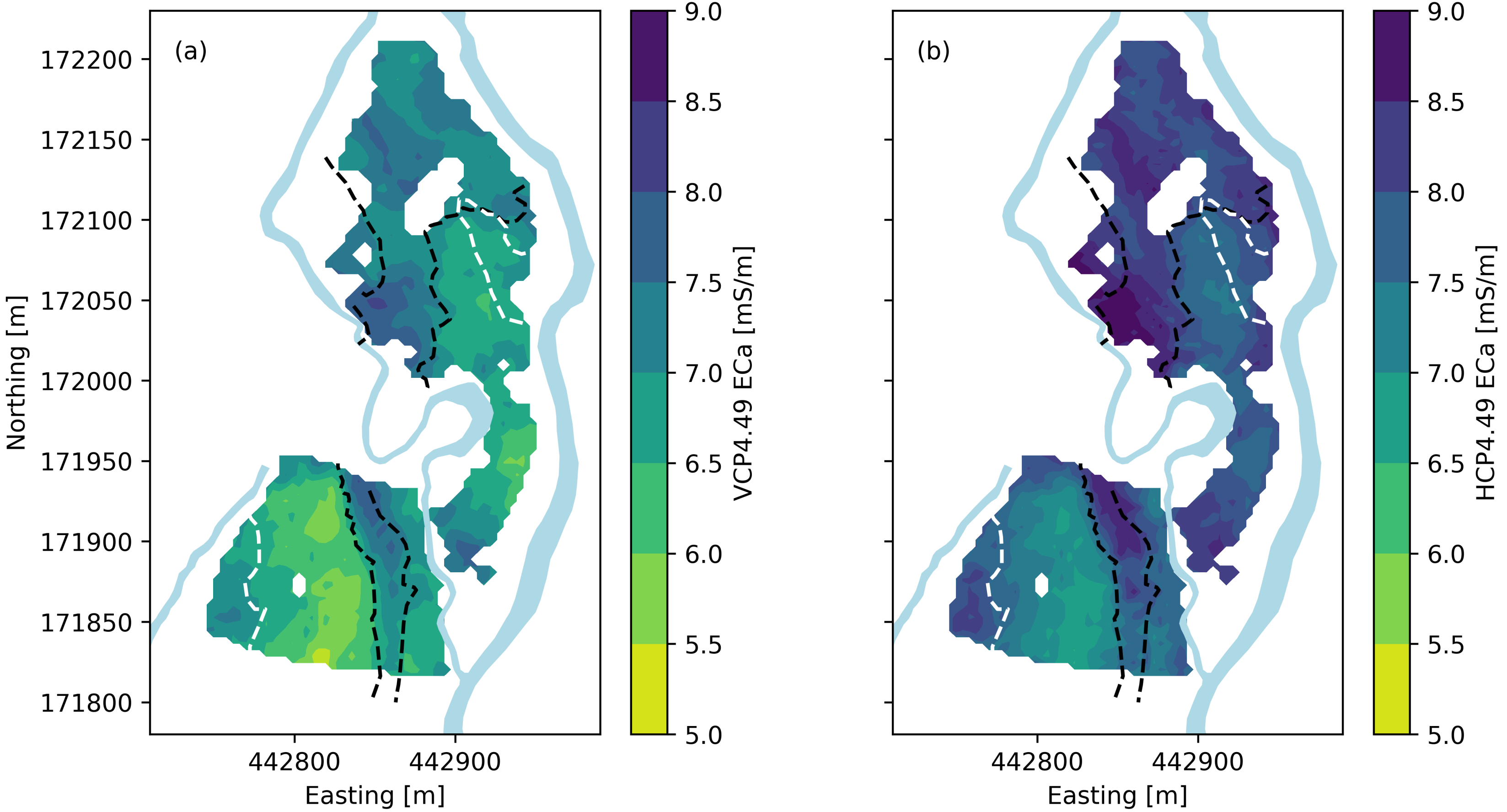
(a)
(b)
Northing [m]
172200
172150
172100
172050
172000
171950
171900
171850
171800
Easting [m]
442800
442900
VCP4.49 ECa [mS/m]
HCP4.49 ECa [mS/m]
9.0
8.5
8.0
7.5
7.0
6.5
6.0
5.5
5.0

Figure6.

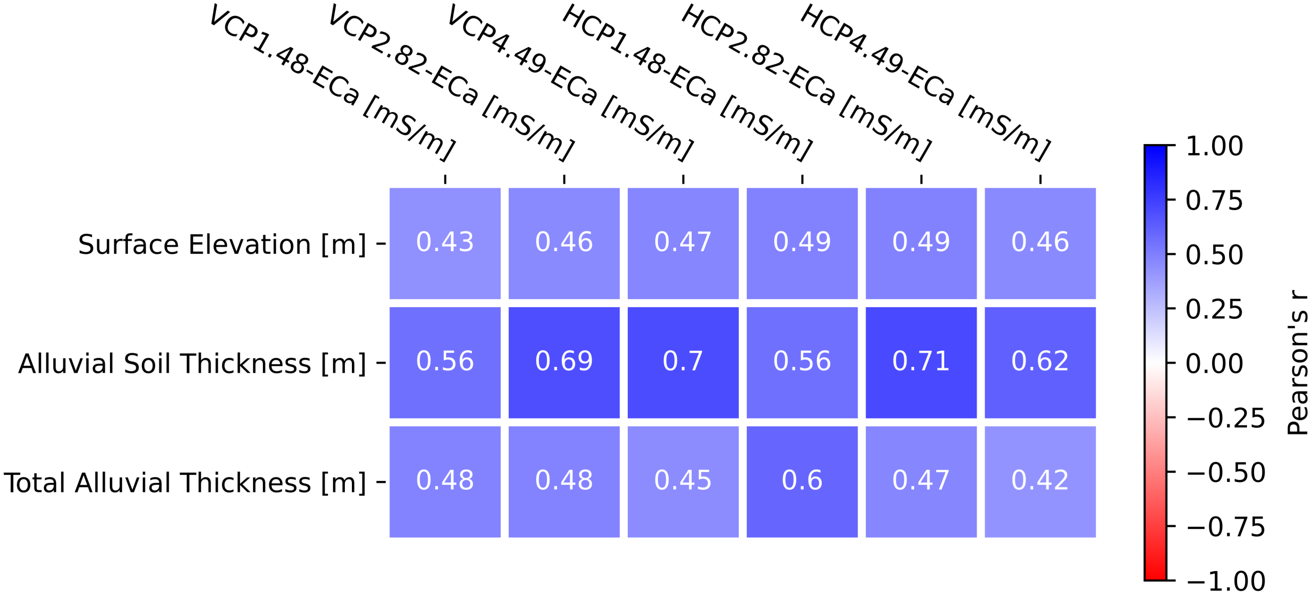
VCP1.48-ECa [mS/m]
VCP2.82-ECa [mS/m]
VCP4.49-ECa [mS/m]
HCP1.48-ECa [mS/m]
HCP2.82-ECa [mS/m]
HCP4.49-ECa [mS/m]
Surface Elevation [m]
0.43
0.46
0.47
0.49
0.49
0.46
Alluvial Soil Thickness [m]
0.56
0.69
0.7
0.56
0.71
0.62
Total Alluvial Thickness [m]
0.48
0.48
0.45
0.6
0.47
0.42
1.00
0.75
0.50
0.25
0.00
−0.25
−0.50
−0.75
−1.00
Pearson's r

Figure7.

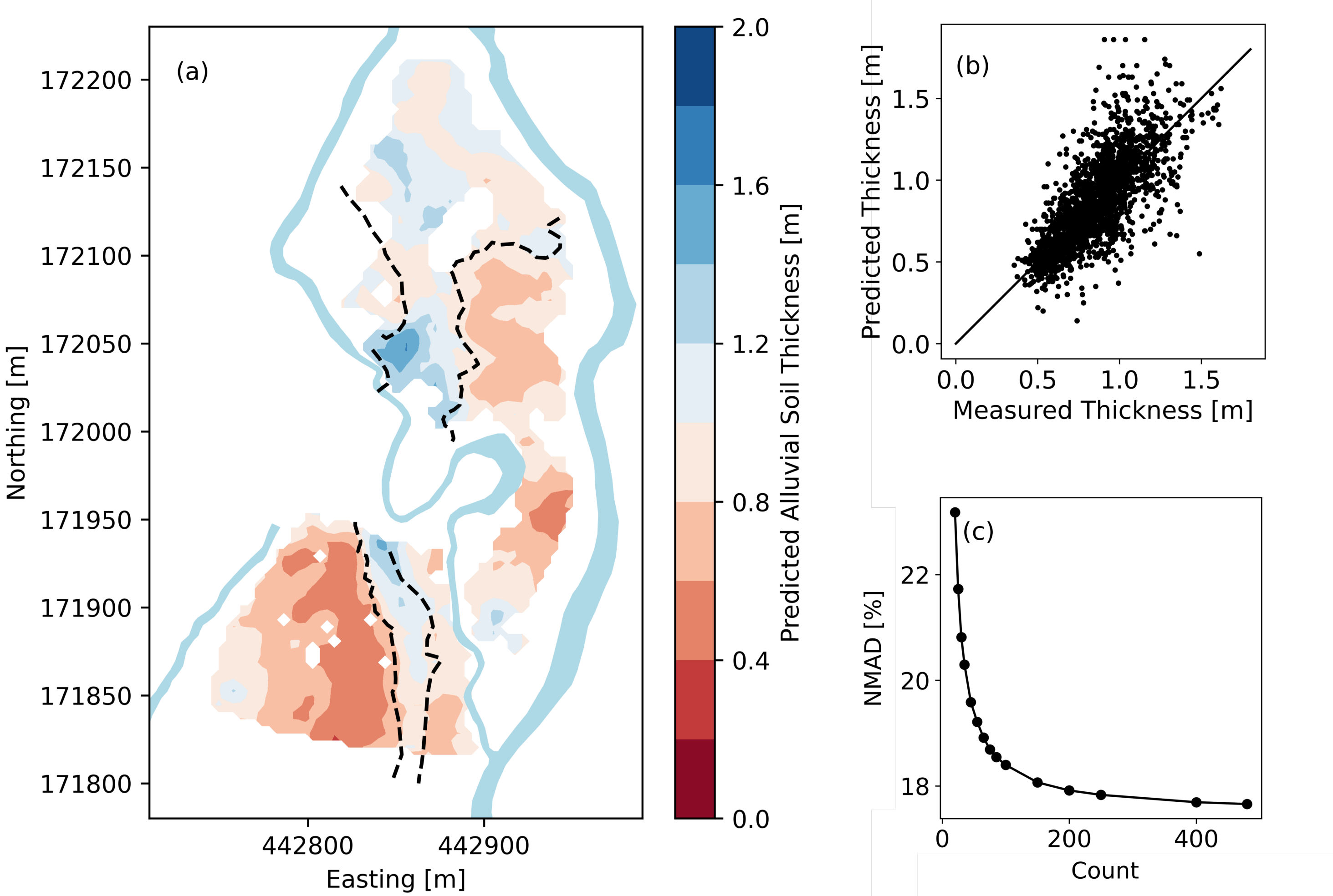

(a)
172200
172150
172100
172050
172000
171950
171900
171850
171800
Northing [m]
442800
442900
Easting [m]
2.0
1.6
1.2
0.8
0.4
0.0
Predicted Alluvial Soil Thickness [m]
(b)
Predicted Thickness [m]
Measured Thickness [m]
0.0
0.5
1.0
1.5
(c)
NMAD [%]
22
20
18
Count
0
200
400

Figure8.

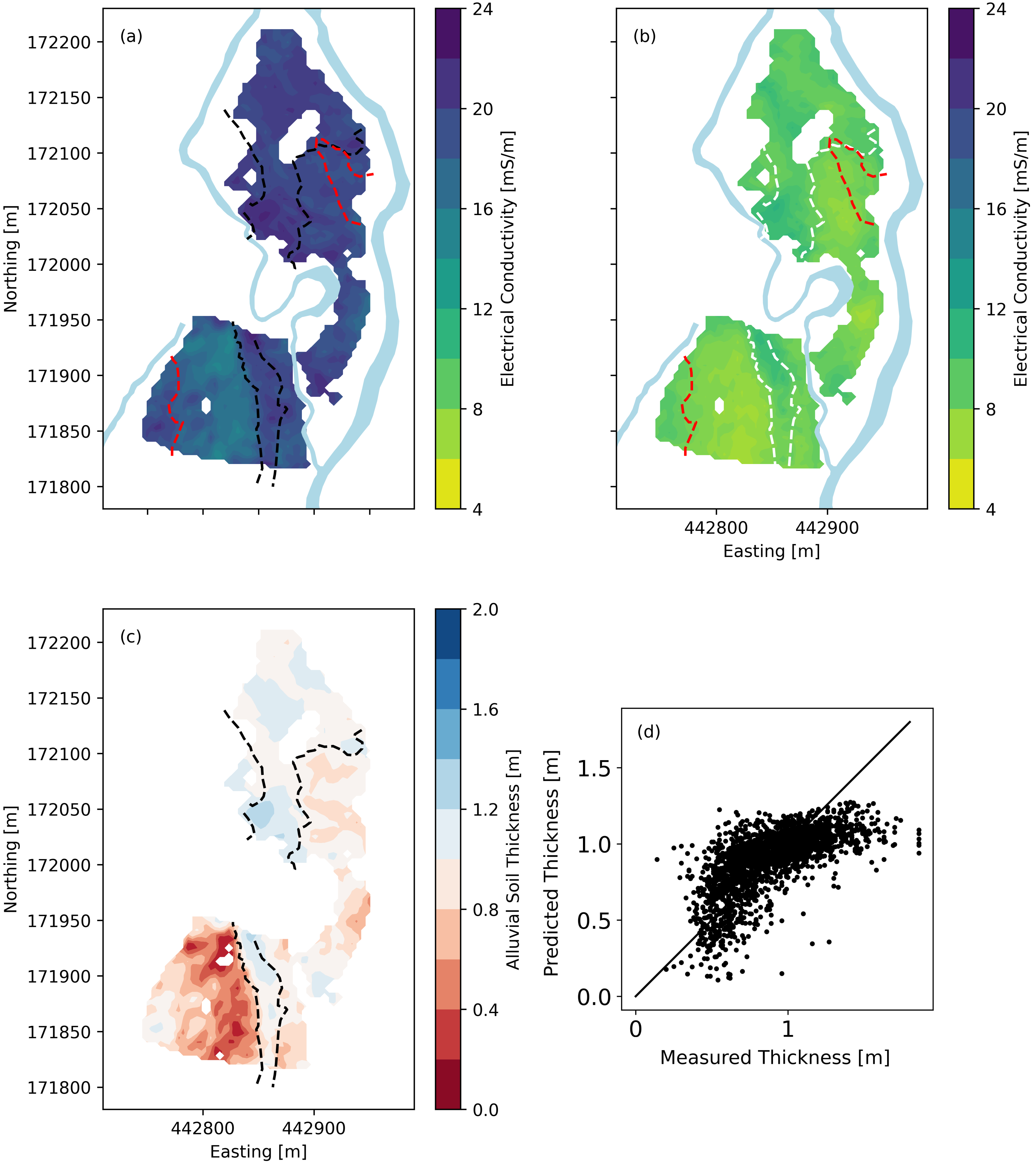

(a)
(b)
(c)
(d)
Northing [m]
Easting [m]
Electrical Conductivity [mS/m]
Alluvial Soil Thickness [m]
Predicted Thickness [m]
Measured Thickness [m]
172200
172150
172100
172050
172000
171950
171900
171850
171800
442800
442900
4
8
12
16
20
24
0.0
0.4
0.8
1.2
1.6
2.0
0.0
0.5
1.0
1.5
0
1

Figure9.

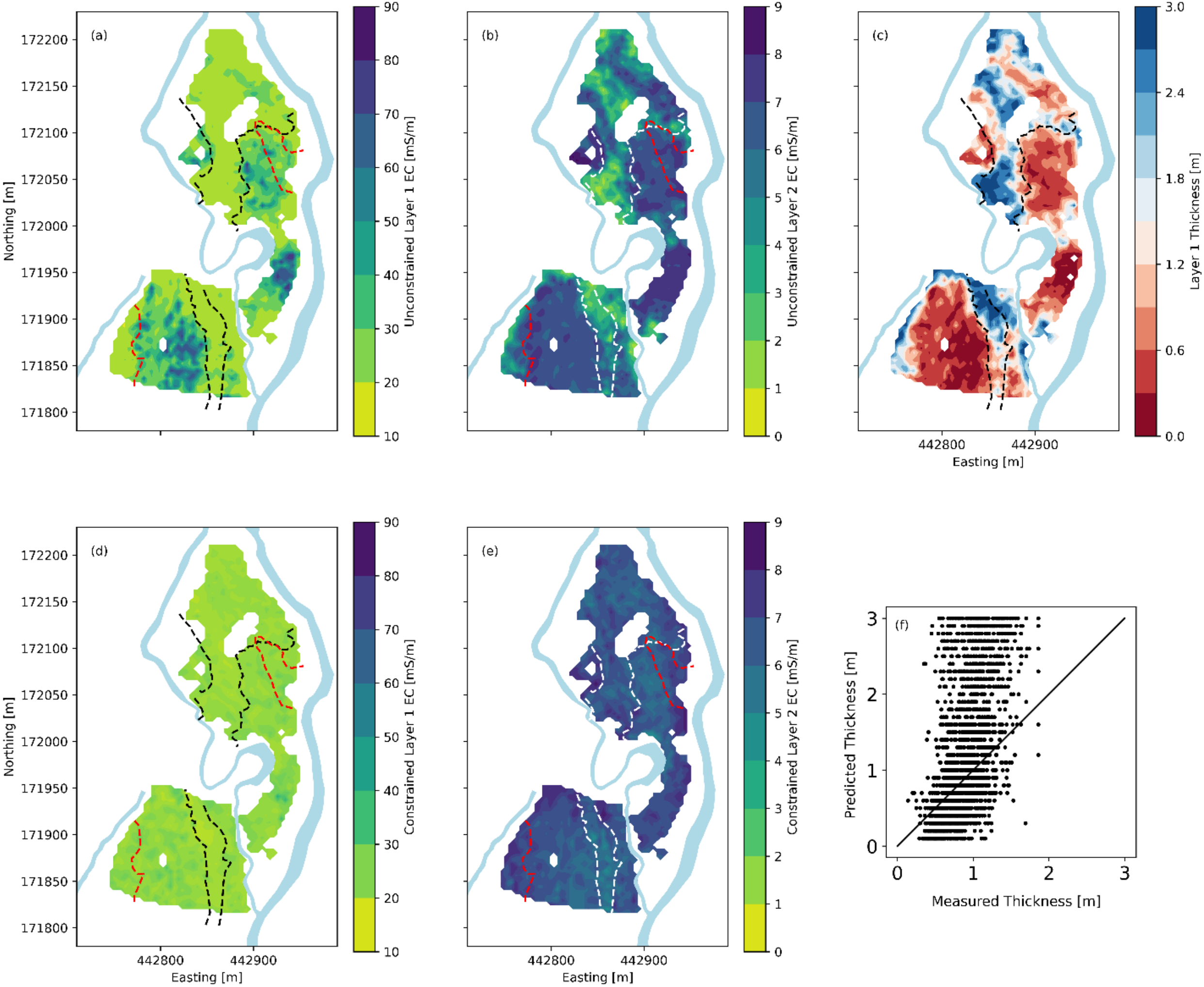
(a)
(b)
(c)
(d)
(e)
(f)
Northing [m]
172200
172150
172100
172050
172000
171950
171900
171850
171800
Easting [m]
442800
442900
Unconstrained Layer 1 EC [mS/m]
Unconstrained Layer 2 EC [mS/m]
Layer 1 Thickness [m]
Constrained Layer 1 EC [mS/m]
Constrained Layer 2 EC [mS/m]
Predicted Thickness [m]
Measured Thickness [m]

Figure10.

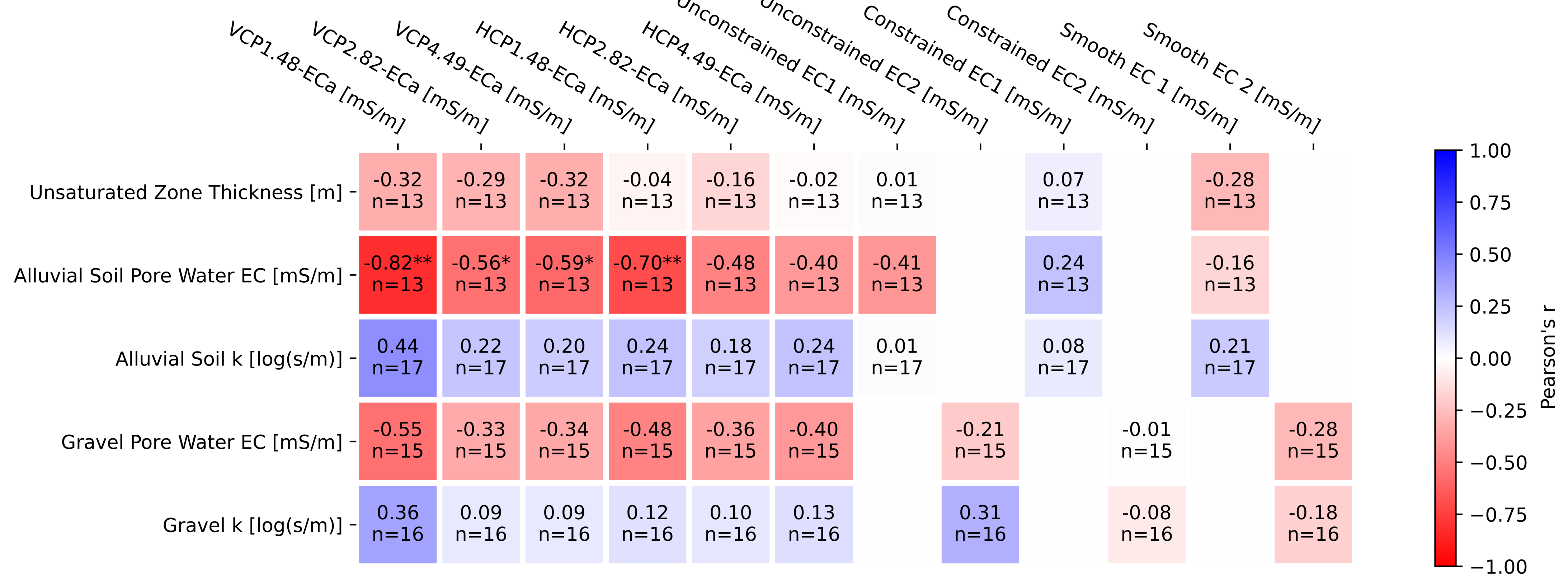
VCP1.48-ECa [mS/m]
VCP2.82-ECa [mS/m]
VCP4.49-ECa [mS/m]
HCP1.48-ECa [mS/m]
HCP2.82-ECa [mS/m]
HCP4.49-ECa [mS/m]
Unconstrained EC1 [mS/m]
Unconstrained EC2 [mS/m]
Constrained EC1 [mS/m]
Constrained EC2 [mS/m]
Smooth EC 1 [mS/m]
Smooth EC 2 [mS/m]
Unsaturated Zone Thickness [m]
Alluvial Soil Pore Water EC [mS/m]
Alluvial Soil k [log(s/m)]
Gravel Pore Water EC [mS/m]
Gravel k [log(s/m)]
-0.32 n=13
-0.29 n=13
-0.32 n=13
-0.04 n=13
-0.16 n=13
-0.02 n=13
0.01 n=13
0.07 n=13
-0.28 n=13
-0.82** n=13
-0.56* n=13
-0.59* n=13
-0.70** n=13
-0.48 n=13
-0.40 n=13
-0.41 n=13
0.24 n=13
-0.16 n=13
0.44 n=17
0.22 n=17
0.20 n=17
0.24 n=17
0.18 n=17
0.24 n=17
0.01 n=17
0.08 n=17
0.21 n=17
-0.55 n=15
-0.33 n=15
-0.34 n=15
-0.48 n=15
-0.36 n=15
-0.40 n=15
-0.21 n=15
-0.01 n=15
-0.28 n=15
0.36 n=16
0.09 n=16
0.09 n=16
0.12 n=16
0.10 n=16
0.13 n=16
0.31 n=16
-0.08 n=16
-0.18 n=16
1.00
0.75
0.50
0.25
0.00
−0.25
−0.50
−0.75
−1.00
Pearson's r